

Higgs production in bottom quark annihilation: Transverse momentum distribution at NNLO+NNLL

Robert V. Harlander^a, Anurag Tripathi^b, Marius Wiesemann^c

^a*Fachbereich C, Bergische Universität Wuppertal,
42097 Wuppertal, Germany*

^b*Dipartimento di Fisica, Università di Torino
and INFN, Sezione di Torino,
10125 Torino, Italy*

^c*Physik-Institut, Universität Zürich,
8057 Zürich, Switzerland*

Abstract

We present the inclusive transverse momentum distribution for Higgs bosons produced in bottom quark annihilation at the LHC. The results are obtained in the five-flavor scheme. The soft and collinear terms at small p_T are resummed through NNLL accuracy and matched to the NNLO transverse momentum distribution at large p_T . We find that the theoretical uncertainty, derived from a variation of the unphysical scales entering the calculation, is significantly reduced with respect to lower orders.

1 Introduction

In the Standard Model (SM), Higgs boson production proceeds predominantly through gluon fusion. The theoretical efforts that went into the precise prediction of the corresponding total cross section as well as kinematical distributions are enormous (see Refs. [1–3] for more information). Other processes such as associated VH or $t\bar{t}H$ production, or weak boson fusion, receive their importance from their characteristic final state particles or kinematics which typically improve the signal-to-background ratio relative to gluon fusion.

Similar to $t\bar{t}H$ production, the Higgs boson can also be produced in association with bottom quarks ($b\bar{b}H$). Until now, however, this process has been largely disregarded in SM Higgs searches and studies, even though its cross section is larger than for $t\bar{t}H$ production [4], since the suppression by the smaller Yukawa coupling is overcompensated by the increased phase space. However, in searches for a SM Higgs boson, the experimental significance of the associated production with bottom quarks suffers heavily from the enormous QCD background.

In theories with an extended Higgs sector, such as the Two-Higgs-Doublet Model (2HDM) or the Minimal Supersymmetric SM (MSSM), the bottom Yukawa coupling can be enhanced relative to the SM so that $b\bar{b}H$ can become the dominant Higgs production mechanism. Concerning the theoretical prediction for this process, mainly two complementary approaches have been pursued in the past. In the *four-flavor scheme* (4FS), the leading-order (LO) partonic processes are $q\bar{q} \rightarrow b\bar{b}H$ and $g\bar{g} \rightarrow b\bar{b}H$, where $q \in \{u, d, c, s\}$. This approach is most suitable when the bottom quarks are considered as part of the signature. The theoretical prediction is available through next-to-LO (NLO) QCD in the 4FS [5–7].

In the *five-flavor scheme* (5FS) at LO, the final state bottom quarks are considered as part of the proton remnants, which are implicitly integrated over in the parton model. The LO process thus becomes $b\bar{b} \rightarrow H$, which needs to be convolved with appropriate b -quark density functions. The $b\bar{b}H$ process evaluated in the 5FS is thus also referred to as *bottom quark annihilation*. This approach is most suitable for the calculation of the $b\bar{b}H$ component to inclusive Higgs production. Its advantage with respect to the 4FS in this case is that, on the one hand, logarithms of the form $\ln m_b/M$ (m_b is the bottom quark mass, M the Higgs mass) which arise from integrating over the collinear region of the final state bottom quark momenta, are implicitly resummed through DGLAP evolution. On the other hand, due to the much simpler structure of the LO process, its theoretical prediction can be obtained at higher perturbative order than for the 4FS. Indeed, the next-to-NLO (NNLO) result for the inclusive total cross section in the 5FS has been known for more than 10 years [8]. The theoretical uncertainty, derived from renormalization and factorization scale variation, is significantly smaller than in the 4FS, in particular, for Higgs masses above 200 GeV. Experimental analyses are currently based on a pragmatic combination of the NLO 4FS and the NNLO 5FS result, as suggested in Ref. [9].

With increasing luminosity, kinematical distributions of the Higgs boson will become more and more important for the clear identification of this particle and the search for possible deviations from the SM predictions. Among the simplest observables in this respect is the transverse momentum (p_T) distribution of the Higgs. Comparison to theoretical predictions will provide a handle to the precise nature of the Higgs couplings, for example to gluons [10–12], where the Higgs-gluon coupling is mediated through a quark loop. Similarly, the associated production of a Higgs with bottom quarks plays a central role to measure the Higgs-bottom Yukawa coupling, in particular in theories where this coupling is enhanced.

It is well known that fixed-order predictions of the p_T spectrum break down for small values of p_T . A proper theoretical description in this region can be obtained by a resummation of logarithmic terms in p_T , leading to a reordering of the perturbative series. At this point, it is useful to clarify our notation for the perturbative orders of the p_T distribution. In gluon fusion as well as in $b\bar{b}H$ within the 5FS, the kinematics of the LO partonic process is $2 \rightarrow 1$, so that the p_T distribution vanishes for $p_T \neq 0$. Quite often one therefore speaks of the “LO p_T distribution” only when an additional parton is emitted which can balance a finite p_T of the Higgs. In this paper, however, we will consistently associate the term “LO” with the $2 \rightarrow 1$ process, so that in our notation, the LO p_T distribution in gluon fusion and 5FS- $b\bar{b}H$ is $\sim \delta(p_T)$.

In gluon fusion, the p_T distribution has been studied in great detail. The NNLO result in the heavy-top limit was presented long ago [13, 14]. Subleading top-mass effects were calculated in Ref. [15]. For the resummation in the small- p_T region, various approaches have been pursued. In Ref. [16], a matching procedure between the resummed next-to-next-to-leading logarithmic (NNLL) terms and the NNLO p_T distribution has been suggested which, when integrated over all p_T , reproduces the total cross section at NNLO. Its application to the gluon fusion process was implemented in the program HqT [16–18], which calculates the NNLO+NNLL p_T spectrum of the Higgs in the limit of an infinitely heavy top mass. The effects of exact top and bottom masses on the resummed transverse momentum distribution were studied at NLO+NLL in Ref. [19, 20].¹

For $b\bar{b}H$, the NNLO p_T spectrum of the Higgs for $p_T > 0$ in the 5FS was obtained in Ref. [23, 24]. The jet- and p_T -vetoed rate [23, 25], as well as the fully differential cross section [26] are also known up to NNLO. The special case of $H+b$ production was considered earlier in Ref. [27]. So far, resummation of the p_T spectrum of the Higgs produced in bottom annihilation has been considered only at NLO+NLL [28]. In this paper, we present the first result of the resummed NNLO+NNLL transverse momentum distribution in the 5FS.

The remainder of the paper is organized as follows: In Section 2.1, we give a brief outline of the p_T resummation formalism for the production of an uncolored final state. This

¹A similar study was pursued in Ref. [21], which additionally discusses the mass effects on the p_T^{veto} cross section, based on the techniques presented in Ref. [22].

section also defines the notation for the rest of the article. Section 2.2 describes the matching procedure to the fixed-order result. In Section 2.3, we present our result for the so-called *hard coefficient* which was the only missing ingredient for the calculation of the resummed p_T distribution at NNLO+NNLL. Our numerical results are presented in Section 3, including a description of the consistency checks that have been performed on the implementation (Section 3.1), the default input parameters (Section 3.2), and finally the p_T distributions (Section 3.3) for the LHC at a center-of-mass energy of 8 TeV (results for 13 TeV are presented in Appendix D). We analyze the dependence of the differential cross section on the unphysical scales and the parton distributions. Section 4 contains our conclusions. In Appendix C, we give complementary information on complex Mellin transforms of some transcendental functions, that appear in our calculation.

2 Transverse momentum resummation

2.1 Elements

For the following discussion, it will be convenient to consider the production of a general colorless particle of mass M with transverse momentum p_T in proton-proton collisions. The specialization to $b\bar{b}H$, where $M = M_H$, will be done in Section 2.3.

If p_T is significantly smaller than M , large logarithms of p_T/M arise in the distribution $d\sigma/dp_T$ due to an incomplete cancellation of soft and collinear contributions. Since each order of perturbation theory introduces additional powers of these logarithms, the naïve perturbative expansion in α_s is no longer valid as $p_T \rightarrow 0$. However, factorization of soft and collinear radiation from the hard process allows us to resum the logarithms to all orders in α_s . This factorization is observed when working in the so-called impact parameter (b) space, defined via the Fourier transformation²

$$f(\mathbf{p}_T) = \frac{1}{(2\pi)^2} \int d^2\mathbf{b} e^{-i\mathbf{b}\cdot\mathbf{p}_T} f(\mathbf{b}), \quad (1)$$

implying that the limit $p_T \rightarrow 0$ corresponds to $b \rightarrow \infty$. Using rotational invariance around the beam axis, the angular integration can be performed, so that we may write the p_T distribution in the form

$$\frac{d\sigma^{F,(\text{res})}}{dp_T^2} = \tau \int_0^\infty db \frac{b}{2} J_0(bp_T) W^F(b, M, \tau), \quad (2)$$

with the Bessel function $J_0(x)$, $\tau = M^2/S$, and S the hadronic center-of-mass energy. By the superscript “(res)” in Eq. (2), we have already indicated that we are going to use

²The momentum conservation relates \mathbf{p}_T to the transverse momenta $\mathbf{K}_T = \sum_i \mathbf{k}_{i,T}$ of the outgoing partons which is factorized in b space using $\delta(\mathbf{p}_T + \mathbf{K}_T) = (2\pi)^{-2} \int d\mathbf{b} \exp[-i\mathbf{b} \cdot \mathbf{p}_T] \exp[-i\mathbf{b} \cdot \mathbf{K}_T]$.

this equation only for $p_T \ll M$, where the logarithmically enhanced terms need to be resummed. The proper inclusion of terms $p_T \gtrsim M$ will be described in Section 2.2. Here and in what follows, the superscript F is attached to process specific quantities; we will set $F = \text{DY}$ for the Drell-Yan production of a vector boson, for example, and $F = b\bar{b}H$ for the $b\bar{b}H$ process.

It is convenient to consider the Mellin transform with respect to the variable τ of the resummed cross section in b space,

$$W_N^F(b, M) = \int_0^1 d\tau \tau^{N-1} W^F(b, M, \tau), \quad (3)$$

which can be written as [29, 31]³

$$\begin{aligned} W_N^F(b, M) &= \sum_c \hat{\sigma}_{c\bar{c}}^{F,(0)} H_c^F(\alpha_s) \\ &\times \exp \left\{ - \int_{b_0^2/b^2}^{M^2} \frac{dk^2}{k^2} \left[A_c(\alpha_s(k)) \ln \frac{M^2}{k^2} + B_c(\alpha_s(k)) \right] \right\} \\ &\times \sum_{i,j} C_{ci,N}(\alpha_s(b_0/b)) C_{\bar{c}j,N}(\alpha_s(b_0/b)) f_{i,N}(b_0/b) f_{j,N}(b_0/b), \end{aligned} \quad (4)$$

where $\hat{\sigma}_{c\bar{c}}^{F,(0)}$ is called the Born factor and determines the parton level cross section at LO. Unless indicated otherwise, the renormalization and factorization scales have been set to $\mu_F = \mu_R = M$. The sum \sum_c runs over all relevant quark flavors $c = q \in \{u, d, s, c, b\}$ and their charge conjugates, as well as gluons, $c = g$ (where $\bar{g} \equiv g$). It takes into account that, already at LO, different initial states can contribute.⁴ In the $b\bar{b}H$ process though, only $c \in \{b, \bar{b}\}$ is relevant, and

$$\hat{\sigma}_{b\bar{b}}^{b\bar{b}H,(0)} = \frac{\pi m_b^2}{6v^2 M^2}, \quad (5)$$

where M is the Higgs mass, m_b the bottom quark mass, and $v \approx 246 \text{ GeV}$ is the vacuum expectation value of the Higgs field. The function $f_{i,N}(q)$ in Eq. (4) is the Mellin transform of the density function $f_i(x, q)$ of parton i in the proton, where x is the momentum fraction and q the momentum transfer. The numerical constant $b_0 = 2 \exp(-\gamma_E)$, with Euler's constant $\gamma_E = 0.5772 \dots$, is introduced for convenience.

The perturbative expansion of the *resummation coefficients* is given by

$$\begin{aligned} C_{ci,N}(\alpha_s) &= \delta_{ci} + \sum_{n=1}^{\infty} \left(\frac{\alpha_s}{\pi} \right)^n C_{ci,N}^{(n)}, & X(\alpha_s) &= \sum_{n=1}^{\infty} \left(\frac{\alpha_s}{\pi} \right)^n X^{(n)}, \\ H_c^F(\alpha_s) &= 1 + \sum_{n=1}^{\infty} \left(\frac{\alpha_s}{\pi} \right)^n H_c^{F,(n)}, \end{aligned} \quad (6)$$

³Throughout this paper, parameters that are not crucial for the discussion will be suppressed in function arguments.

⁴For example, the LO DY process receives contributions from all light quark flavors.

where $X \in \{A_c, B_c\}$. The order at which these coefficients are taken into account in Eq. (4) determines the *logarithmic accuracy* of the resummed cross section; *leading logarithmic* (LL) means that all higher order coefficients except for $A_c^{(1)}$ are neglected, *next-to-LL* (NLL) requires $A_c^{(2)}$, $B_c^{(1)}$, $C_{ci}^{(1)}$, and $H_c^{F,(1)}$, etc. The coefficients required for the $b\bar{b}H$ process at next-to-NLL (NNLL) accuracy are given in Section 2.3.

The fact that the coefficients A_c , B_c , and C_{ci} in Eq. (4) are process independent (i.e., they do not carry a superscript F) assumes a common *resummation scheme*⁵ for all ($c\bar{c}$ initiated, $c \in \{g, q\}$) processes F . The entire process dependence is then contained in the *hard coefficient* H_c^F and the Born factor $\hat{\sigma}_{c\bar{c}}^{F,(0)}$. In the following, we will work in the *DY scheme*, where $H_q^{\text{DY}} \equiv 1$ through all orders of perturbation theory. All resummation coefficients are known in the DY scheme up to the order required in this paper (see Section 2.3), with the exception of $H_b^{b\bar{b}H} \equiv H_b^H$ whose evaluation through NNLO will also be presented in Section 2.3.

Evolving the parton densities from b_0/b to μ_F in Eq. (4) (see Ref. [16]), one can define the partonic resummed cross section $\mathcal{W}_{ij,N}^F$ through

$$W_N^F(b, M) = \sum_{i,j} \mathcal{W}_{ij,N}^F(b, M, \mu_F) f_{i,N}(\mu_F) f_{j,N}(\mu_F). \quad (7)$$

From a perturbative point of view, \mathcal{W}^F can be cast into the form

$$\mathcal{W}_{ij,N}^F(b, M, \mu_F) = \sum_c \hat{\sigma}_{c\bar{c}}^{F,(0)} \left\{ \mathcal{H}_{c\bar{c} \leftarrow ij,N}^F(M, Q, \mu_F) + \Sigma_{c\bar{c} \leftarrow ij,N}^F(L, M, Q, \mu_F) \right\}, \quad (8)$$

where $L = \ln(Q^2 b^2 / b_0^2)$ denotes the logarithms that are being resummed in \mathcal{W}^F , and Q is an arbitrary *resummation scale*. While \mathcal{W}^F is formally independent of Q , truncation of the perturbative series will introduce a dependence on this scale which is, however, of higher order. The variation of the cross section with Q will be taken into account when estimating the theoretical uncertainty of our final result in Section 3.3. Note that the entire b dependence, parametrized in terms of L , is contained in the functions $\Sigma_{c\bar{c} \leftarrow ij}^F$ which are *defined* to vanish at $L = 0$. Their generic perturbative expansion through NNLO, expressed in terms of the resummation coefficients of Eq. (6), can be found in Ref. [16]. The *hard-collinear function* $\mathcal{H}_{c\bar{c} \leftarrow ij}^F$ depends on the coefficients H_c^F and C_{ci} of Eq. (4). For $\mu_F = \mu_R = Q = M$ and $c \neq g$ (for $c = g$, see Ref. [32])

$$\mathcal{H}_{c\bar{c} \leftarrow ij,N}^F = H_c^F(\alpha_s) C_{ci,N}(\alpha_s) C_{\bar{c}j,N}(\alpha_s), \quad (9)$$

where $\alpha_s \equiv \alpha_s(M)$. The expression for $\mathcal{H}_{c\bar{c} \leftarrow ij}^F$ for the $b\bar{b}H$ process including the full scale dependence through NNLO is given in Eq. (29).

⁵See Ref. [16] for details.

Recalling that the formalism discussed in this section is valid only in the small- p_T region, it is convenient to replace [16]

$$L \rightarrow \tilde{L} \equiv \ln \left(\frac{Q^2 b^2}{b_0^2} + 1 \right), \quad (10)$$

in the resummed cross section, which will prove useful in the next section to suppress the impact of $\Sigma_{c\bar{c} \leftarrow ij}^F$ in the large- p_T region without affecting the logarithmic accuracy under consideration. Note, however, that this replacement changes the Q dependence of $\Sigma_{c\bar{c} \leftarrow ij}^F$, so that Eq. (8)—and therefore $d\sigma^{(\text{res})}/dp_T^2$ —becomes explicitly Q dependent. We will come back to this issue in the next section.

2.2 Matching with the large- p_T region

In the previous section we recalled the formalism of transverse momentum resummation at small p_T . In order to obtain a result that is valid for arbitrary values of p_T , a matching to the distribution at high values of p_T is required, which is predominantly given by the fixed-order result. We will follow the additive matching procedure of Ref. [16], where the resummed-matched result $[d\sigma]_{\text{f.o.}+\text{l.a.}}$ is obtained by subtracting from the fixed-order distribution $[d\sigma]_{\text{f.o.}}$ the logarithms at $p_T \rightarrow 0$ at the same order in α_s , and adding the resummed expression at the appropriate logarithmic accuracy $[d\sigma^{(\text{res})}]_{\text{l.a.}}$:

$$\left[\frac{d\sigma^F}{dp_T^2} \right]_{\text{f.o.}+\text{l.a.}} = \left[\frac{d\sigma^F}{dp_T^2} \right]_{\text{f.o.}} - \left[\frac{d\sigma^{F,(\text{res})}}{dp_T^2} \right]_{\text{f.o.}} + \left[\frac{d\sigma^{F,(\text{res})}}{dp_T^2} \right]_{\text{l.a.}}. \quad (11)$$

The logarithmic terms $[d\sigma^{(\text{res})}]_{\text{f.o.}}$ are obtained from the perturbative expansion of Eq. (2). The matching condition is imposed by requiring

$$\left[\left[\frac{d\sigma^{F,(\text{res})}}{dp_T^2} \right]_{\text{l.a.}} \right]_{\text{f.o.}} = \left[\frac{d\sigma^{F,(\text{res})}}{dp_T^2} \right]_{\text{f.o.}}, \quad (12)$$

which defines the logarithmic accuracy needed at each perturbative order in α_s and vice versa. Thus, at a given order in α_s , it determines to which order the resummation coefficients of Eq. (6) are required. Note that the Q dependence of $d\sigma^{(\text{res})}$ introduced by the replacement $L \rightarrow \tilde{L}$ of Eq. (10) cancels up to higher orders in Eq. (11).

Integrating Eq. (2) (with $L \rightarrow \tilde{L}$) over p_T^2 by using $\int dp_T^2 J_0(bp_T) = \pi\delta(b^2)$ (or elementary properties of the Fourier transform) and $\Sigma_{c\bar{c} \leftarrow ij}(\tilde{L} = 0) = 0$, it directly follows that

$$\int dp_T^2 \frac{d\sigma^{F,(\text{res})}}{dp_T^2} = \tau \sum_{c,i,j} \hat{\sigma}_{c\bar{c}}^{F,(0)} (\mathcal{H}_{c\bar{c} \leftarrow ij}^F \otimes f_i \otimes f_j)(\tau), \quad (13)$$

where the convolution of two functions h_1 and h_2 is defined as

$$(h_1 \otimes h_2)(\tau) \equiv \int_0^1 dz_1 \int_0^1 dz_2 \delta(\tau - z_1 z_2) h_1(z_1) h_2(z_2). \quad (14)$$

Needless to say, f_i and $\mathcal{H}_{c\bar{c} \leftarrow ij}^F$ in Eq. (13) denote the inverse Mellin transforms of $f_{i,N}$ and $\mathcal{H}_{c\bar{c} \leftarrow ij,N}^F$.

For the r.h.s. of Eq. (13), it is $[\cdot]_{\text{f.o.}} = [[\cdot]_{\text{l.a.}}]_{\text{f.o.}}$; using Eq. (12), it is thus easy to see that the integral over p_T^2 is the same for $[d\sigma^{(\text{res})}]_{\text{f.o.}}$ and $[d\sigma^{(\text{res})}]_{\text{l.a.}}$. One therefore obtains a *unitarity constraint* on the resummed-matched cross section which implies that the integral over p_T^2 reproduces the total cross section σ_{tot} at fixed order:⁶

$$\int dp_T^2 \left[\frac{d\sigma^F}{dp_T^2} \right]_{\text{f.o.}+\text{l.a.}} \equiv [\sigma_{\text{tot}}^F]_{\text{f.o.}}. \quad (15)$$

This relation will be used in Section 2.3 to determine the second-order coefficient of the hard function H_b^H numerically, which is the only missing piece for carrying out the full NNLL p_T resummation for the $b\bar{b}H$ process in the 5FS.

2.3 Resummation coefficients and determination of $H_b^{H,(2)}$

In the DY scheme, the resummation coefficients relevant for the $b\bar{b}H$ process read

$$\begin{aligned} A_b^{(1)} &= C_F, & A_b^{(2)} &= \frac{1}{2} C_F \left[\left(\frac{67}{18} - \frac{\pi^2}{6} \right) C_A - \frac{5}{9} N_f \right], \\ A_b^{(3)} &= C_A^2 C_F \left(\frac{11\pi^4}{720} - \frac{67\pi^2}{216} + \frac{245}{96} + \frac{11}{24} \zeta_3 \right) + C_A C_F N_f \left(\frac{5\pi^2}{108} - \frac{209}{432} - \frac{7}{12} \zeta_3 \right) \\ &\quad + C_F^2 N_f \left(-\frac{55}{96} + \frac{1}{2} \zeta_3 \right) - \frac{1}{108} C_F N_f^2 + 8\beta_0 C_F \left(C_A \left(\frac{101}{216} - \frac{7}{16} \zeta_3 \right) - \frac{7}{108} N_f \right) \\ B_b^{(1)} &= -\frac{3}{2} C_F, & B_b^{(2)} &= \frac{C_F}{4} \left[C_F \left(\pi^2 - \frac{3}{4} - 12\zeta_3 \right) + C_A \left(\frac{11}{9} \pi^2 - \frac{193}{12} + 6\zeta_3 \right) \right. \\ &\quad \left. + N_f \left(\frac{17}{6} - \frac{2}{9} \pi^2 \right) \right], \end{aligned} \quad (16)$$

where $\beta_0 = (11 C_A - 2 N_f)/12$, $C_F = 4/3$, $C_A = 3$, and $N_f = 5$ is the number of active quark flavors; furthermore $\zeta_3 \equiv \zeta(3) = 1.20206\dots$ with Riemann's ζ function. $A_c^{(n)}$ and $B_c^{(1)}$ are actually resummation scheme independent. Through $n \in \{1, 2\}$, their expressions

⁶Note that this line of argumentation assumes that terms proportional to $\delta(p_T^2)$ are included in $[d\sigma^{F,(\text{res})}]_{\text{f.o.}}$ as well as $[d\sigma^F]_{\text{f.o.}}$ (implying also that logarithms are actual plus-distributions). In the practical application of Eq. (11), however, these terms cancel and can be disregarded.

have been known for some time [33,34], while $A^{(3)}$ has recently been calculated in Ref. [35]. The coefficient $B_b^{(2)}$ was first obtained in Ref. [36].

The C coefficients which arise in our calculation are of the form $C_{bi}^{(n)}$ ($n \leq 2$), the index b denotes the bottom quark, and $i \in \{u, d, s, c, b, g\}$. Of course, the respective coefficients for the charge conjugate partons are also implied in this notation. In z space (i.e., inverse Mellin space), the first-order coefficients in the DY scheme read [36]

$$\begin{aligned} C_{bg}^{(1)}(z) &= \frac{1}{2} z(1-z), & C_{bq}^{(1)}(z) &= C_{bb}^{(1)}(z) = 0, \\ C_{bb}^{(1)}(z) &= \frac{C_F}{2} \left[\left(\frac{\pi^2}{2} - 4 \right) \delta(1-z) + 1 - z \right]. \end{aligned} \quad (17)$$

The off-diagonal NLO coefficients $C_{bg}^{(1)}, C_{bq}^{(1)}, C_{bb}^{(1)}$ ($q \in \{u, d, s, c\}$) are resummation scheme independent. The second-order coefficients $C_{bi}^{(2)}$ can be found in Ref. [37].

Finally, we need to determine the hard coefficient H_b^H for the bottom annihilation process in the DY scheme. At NLO, it can easily be deduced from the first-order C coefficient in the DY scheme [36] and in the $b\bar{b}H$ scheme [24],⁷ leading to $H_b^{H,(1)} = 3C_F$. On the other hand, we have calculated the NNLO term $H_b^{H,(2)}$ in two independent ways.

Numerical evaluation. Using Eqs. (11), (13) and (15), one finds

$$\tau \sum_{ij} \hat{\sigma}_{bb}^{b\bar{b}H,(0)} ([\mathcal{H}_{bb \leftarrow ij}^{b\bar{b}H}]_{\text{f.o.}} \otimes f_i \otimes f_j)(\tau) = [\sigma^{(\text{tot})}]_{\text{f.o.}} - \int dp_T^2 \left[\frac{d\sigma^{(\text{fin})}}{dp_T^2} \right]_{\text{f.o.}}, \quad (18)$$

where $[d\sigma^{(\text{fin})}]_{\text{f.o.}} \equiv [d\sigma]_{\text{f.o.}} - [d\sigma^{(\text{res})}]_{\text{f.o.}}$. Eq. (18) holds order by order in α_s and for each channel⁸ separately.

If we consider $ij = b\bar{b}$ at $\mathcal{O}(\alpha_s^2)$, the only unknown in Eq. (18) is the hard coefficient $H_b^{H,(2)}$, which appears as a constant in the hard-collinear function $\mathcal{H}_{bb \leftarrow ij}^{b\bar{b}H,(2)}$ (see Eq. (29)). The full z dependence of the latter is known from the C functions in the DY scheme. Thus, we can simply fit $H_b^{H,(2)}$ using Eq. (18) without any approximations. The numerical result we obtain is

$$H_b^{H,(2)} = 10.47 \pm 0.08, \quad (19)$$

where the relatively big uncertainty is caused by the cancellation of several digits on the right-hand side of Eq. (18).

⁷A general result for $C_{ij}^{(1)}$ as a function of the finite part of the one-loop corrections has also been known for some time [38].

⁸As usual, the individual partonic subprocesses (channels) ij are defined according to the $\overline{\text{MS}}$ factorization scheme.

Analytic evaluation. The evaluation of the hard coefficient requires the knowledge of the purely virtual amplitude for the process $b\bar{b}H$ which was calculated through NNLO in Refs. [8,39]. We give below the UV renormalized⁹ $b\bar{b}H$ form factor in $d = 4 - 2\epsilon$ dimensions for $\mu_R = M$, where here and in what follows, M denotes the Higgs boson mass M_H .

$$F_b^h = \tilde{F}_b^h + \hat{F}_b^h, \quad (20)$$

where

$$\begin{aligned} \hat{F}_b^h = & \left(\frac{\alpha_s}{\pi} \right) C_F \left[-\frac{1}{2\epsilon^2} - \frac{1}{\epsilon} \left(\frac{i\pi}{2} + \frac{3}{4} \right) + \frac{\pi^2}{24} \right] + \left(\frac{\alpha_s}{\pi} \right)^2 \left[C_F^2 \left\{ \frac{1}{8\epsilon^4} + \frac{1}{\epsilon^3} \left(\frac{i\pi}{4} + \frac{3}{8} \right) \right. \right. \\ & + \frac{1}{\epsilon^2} \left(\frac{3i\pi}{8} - \frac{13\pi^2}{48} + \frac{17}{32} \right) + \frac{1}{\epsilon} \left(-\frac{5i\pi^3}{24} + \frac{i\pi}{2} - \frac{4\zeta(3)}{3} - \frac{5\pi^2}{32} + \frac{53}{64} \right) - \frac{7i\pi\zeta(3)}{6} \\ & + \frac{11i\pi}{8} - \frac{3i\pi^3}{32} - \frac{7\zeta(3)}{8} + \frac{83\pi^4}{960} - \frac{5\pi^2}{12} + \frac{7}{4} \left. \right\} + C_A C_F \left\{ \frac{11}{32\epsilon^3} + \frac{1}{\epsilon^2} \left(\frac{11i\pi}{48} + \frac{\pi^2}{96} + \frac{1}{9} \right) \right. \\ & + \frac{1}{\epsilon} \left(\frac{i\pi^3}{48} - \frac{67i\pi}{144} + \frac{13\zeta(3)}{16} - \frac{11\pi^2}{192} - \frac{961}{1728} \right) + \frac{11i\pi^3}{288} + \frac{77\zeta(3)}{144} - \frac{\pi^4}{288} \\ & + \frac{67\pi^2}{576} - \frac{607}{648} \left. \right\} + N_f C_F \left\{ -\frac{1}{16\epsilon^3} + \frac{1}{\epsilon^2} \left(-\frac{i\pi}{24} - \frac{1}{36} \right) + \frac{1}{\epsilon} \left(\frac{5i\pi}{72} + \frac{\pi^2}{96} + \frac{65}{864} \right) \right. \\ & \left. \left. - \frac{i\pi^3}{144} - \frac{7\zeta(3)}{72} - \frac{5\pi^2}{288} + \frac{41}{324} \right\} \right] \end{aligned} \quad (21)$$

and

$$\begin{aligned} \tilde{F}_b^h = & 1 + \frac{\alpha_s}{\pi} C_F \left(\frac{\pi^2}{4} - \frac{1}{2} \right) + \left(\frac{\alpha_s}{\pi} \right)^2 \left[C_A C_F \left(\frac{37\zeta_3}{72} + \frac{83}{144} + \frac{125\pi^2}{432} - \frac{\pi^4}{480} \right) \right. \\ & + C_F^2 \left(-\frac{15\zeta_3}{8} + \frac{3}{8} + \frac{\pi^2}{24} + \frac{23\pi^4}{1440} \right) + C_F N_f \left(\frac{\zeta_3}{9} + \frac{1}{36} - \frac{5\pi^2}{108} \right) \\ & \left. + i\pi \left(C_A C_F \left(\frac{13\zeta_3}{8} - \frac{121}{216} - \frac{11\pi^2}{288} \right) + C_F^2 \left(\frac{\pi^2}{8} - \frac{3\zeta_3}{2} \right) + \left(\frac{7}{54} + \frac{\pi^2}{144} \right) C_F N_f \right) \right], \end{aligned} \quad (22)$$

with $\alpha_s = \alpha_s(M)$. All singular terms are contained in \hat{F}_b^h , while \tilde{F}_b^h remains independent of singularities. Note, however, that \hat{F}_b^h also contains finite terms. The splitting has been done according to Ref. [40]. The hard coefficient in the *hard scheme* at $\mu_R = M$ is then obtained at each order in α_s through [40]

$$H_{b,\text{hard}}^H(\alpha_s) = \left| \tilde{F}_b^h(\alpha_s) \right|^2. \quad (23)$$

⁹Both α_s and m_b are renormalized in the $\overline{\text{MS}}$ scheme. In particular, we replace α_s in the whole amplitude according to Eq. (6) of Ref. [39].

Using the fact that scheme conversion is process independent, i.e.,

$$H_{c,\text{hard}}^F = (1 + \Delta_{\text{hard}}) H_c^F, \quad (24)$$

with an appropriate perturbative factor $\Delta_{\text{hard}} = \mathcal{O}(\alpha_s)$, and that $H_q^{\text{DY}}(\alpha_s) \equiv 1$, the conversion to the DY scheme is easily carried out using

$$\begin{aligned} H_b^{H,(1)} &= H_{b,\text{hard}}^{H,(1)} - H_{b,\text{hard}}^{\text{DY},(1)}, \\ H_b^{H,(2)} &= H_{b,\text{hard}}^{H,(2)} - H_{b,\text{hard}}^{\text{DY},(2)} + (H_{b,\text{hard}}^{\text{DY},(1)})^2 - H_{b,\text{hard}}^{H,(1)} H_{b,\text{hard}}^{\text{DY},(1)}, \end{aligned} \quad (25)$$

where $H_{b,\text{hard}}^{\text{DY}}$ is the hard coefficient for the DY process in the hard scheme which is presented in Ref. [40]. In this way we find

$$\begin{aligned} H_b^{H,(2)} &= C_F \left[\left(\frac{321}{64} - \frac{13}{48} \pi^2 \right) C_F + \left(-\frac{365}{288} + \frac{\pi^2}{12} \right) N_f \right. \\ &\quad \left. + \left(\frac{5269}{576} - \frac{5}{12} \pi^2 - \frac{9}{4} \zeta_3 \right) C_A \right]. \end{aligned} \quad (26)$$

This yields a numerical value of $H_b^{H,(2)} = 10.52 \dots$, which is in perfect agreement with Eq. (19). This serves as an important check of our calculation.

3 Outline of the calculation and results

We are now ready to consider the resummed transverse momentum distribution of the Higgs boson produced via bottom quark annihilation through NNLO+NNLL. Exemplary Feynman diagrams that enter our calculation are shown in Appendix A. The LO diagram in Fig. 11 (a) determines the Born factor given in Eq. (5). The virtual one- and two-loop corrections (e.g. Fig. 11 (b) and (c)) govern the hard coefficient H_b^H as outlined in Section 2.3. Fig. 12 shows a sample of real and mixed real-virtual diagrams that appear at NNLO for $p_T > 0$. Note that the various subprocesses enter the calculation at different orders. The $b\bar{b}$ initial state is the only subprocess present at LO. At NLO the contribution of the bg channel also has to be taken into account.¹⁰ The gg -, bb -, bq - and $q\bar{q}$ -initiated subprocesses ($q \in \{u, d, s, c\}$) enter only at NNLO. The only subprocess which is finite at small transverse momenta and needs no resummation is the $q\bar{q}$ channel.

The calculation of the resummed-matched distribution of Eq. (11) requires the differential cross section¹¹ $d\sigma$ calculated in various approximations:

¹⁰We account all charge conjugated and switched initial states to the same subprocess. Thus, the bg channel includes bg , $\bar{b}g$, gb and $g\bar{b}$.

¹¹The superscript $F=b\bar{b}H$ will be dropped in what follows.

- The analytic transverse momentum distribution at NNLO, $[\mathrm{d}\sigma]_{\text{f.o.}}$, can be taken from Ref. [24] (for $p_T > 0$, but see footnote 6).
- The logarithms at NNLO, $[\mathrm{d}\sigma^{(\text{res})}]_{\text{f.o.}}$, are obtained from the fixed-order expansion of $\mathrm{d}\sigma^{(\text{res})}$ which was carried out explicitly in Eqs. (72) and (73) of Ref. [16] (again, only $p_T > 0$ terms are taken into account).¹²
- For the calculation of the resummed expression, $[\mathrm{d}\sigma^{(\text{res})}]_{\text{l.a.}}$, we use a modified version of the program **HqT** [16–18], which performs the transverse momentum resummation for gluon-induced Higgs production in the heavy-top limit. We extended its capabilities to also cover the resummation for quark-induced processes and implemented the resummation coefficients of the $b\bar{b}H$ process.

3.1 Checks

Before presenting numerical results, we comment on various checks that we made on our calculation and outline our default input parameters. The analytic p_T distribution at NNLO [24] has been checked numerically against the partonic Monte Carlo program for H +jet production at the same order of Refs. [23, 25], which in turn has been validated by various related calculations¹³ [27, 42–45].

The small- p_T behavior of the distribution needs to agree with the expansion of $\mathrm{d}\sigma^{(\text{res})}$. We checked that the limit

$$\left[\frac{\mathrm{d}\sigma}{\mathrm{d}p_T^2} \right]_{\text{f.o.}} \xrightarrow{p_T \rightarrow 0} \left[\frac{\mathrm{d}\sigma^{(\text{res})}}{\mathrm{d}p_T^2} \right]_{\text{f.o.}} \quad (27)$$

holds to better than one per-mille in the interval $0.001 \text{ GeV} < p_T < 0.1 \text{ GeV}$. We also verified that this limit is independent of the resummation scale.

Furthermore, we used our implementation of $\mathrm{d}\sigma^{(\text{res})}$ to calculate a large number of sampling points in order to approximate the integral over p_T . According to Eq. (13), the result has to yield the (analytically known) hard-collinear function $\mathcal{H}_{b\bar{b} \leftarrow ij}^{b\bar{b}H}$, which we verified up to an accuracy of a few per-mille.¹⁴ This is quite remarkable, considering the fact that the determination of $\mathrm{d}\sigma^{(\text{res})}$ includes the numerical transform from b to p_T space and from N to z space, as well as a fit of the parton distributions in Mellin space.

We also checked Eq. (15) for the resummed-matched cross section up to a numerical accuracy considerably better than one per-mille, using the analytical result for $\mathcal{H}_{b\bar{b} \leftarrow ij}^{b\bar{b}H}$ as the

¹²The corresponding coefficients are given in Eqs. (63), (64), (66), (67), (68) and (69) of Ref. [16].

¹³For more details see also Ref. [41].

¹⁴More precisely, to verify Eq. (13) we used resummation scales significantly smaller than the mass of the Higgs to reduce the impact of resummation at high transverse momenta, because at very high p_T ($p_T \gtrsim 300 \text{ GeV}$) the numerical convergence of our implementation of $\mathrm{d}\sigma^{(\text{res})}$ deteriorates.

integral of $d\sigma^{(\text{res})}$. This was already expected from the agreement between Eq.(19) and the analytical result of Eq. (26) for $H_b^{H,(2)}$ mentioned above.

All these checks have been performed for various values of the resummation, factorization, and renormalization scale, separately at order α_s and α_s^2 , and for the individual partonic subchannels.

At NLO+NLL, the p_T spectrum of the Higgs in $b\bar{b}H$ has already been studied in Ref. [28] within the formalism of Refs. [29,30]. Although their approach—in particular, the matching procedure—differs from ours, the qualitative behavior of our curves is in fairly good agreement at this order. In particular, we find the same properties of the resummed-matched curve at high transverse momenta, which is nontrivial as will be shown in Section 3.3.

3.2 Input parameters

We present results for the LHC at 8 and 13 TeV center-of-mass energy. Our choice for the central factorization and renormalization scale is $\mu_F = \mu_R = \mu_0 \equiv M$; our default value for the resummation scale is $Q = Q_0 \equiv M/4$. If not stated otherwise, all numbers are obtained with the MSTW2008 [46] PDF set, which implies that the input value for the strong coupling constant is taken as $\alpha_s(M_Z) = 0.12018$ at NLO, and $\alpha_s(M_Z) = 0.11707$ at NNLO. For comparison we also report results for the NNPDF2.3 and CT10 PDF sets, with their corresponding $\alpha_s(M_Z)$ values. Since we are working in the 5FS, the bottom mass is set to zero throughout the calculation, except for the bottom-Higgs Yukawa coupling which we insert in the $\overline{\text{MS}}$ scheme at the scale μ_R , derived from the input value $m_b(m_b) = 4.16$ GeV.

All numbers are evaluated within the framework of the SM. Through appropriate rescaling of the bottom Yukawa coupling, they are obviously also applicable to neutral (CP even and odd) Higgs production within the 2HDM and, according to the studies of Refs. [47,48], even within the MSSM.

Sources of theoretical uncertainty and their impact on the numerical results will be studied in Section 3.3. As usual, the uncertainty due to the truncation of the perturbative series with respect to α_s will be estimated from the dependence of the cross section on the unphysical scales μ_F and μ_R . Similarly, the effect of a finite logarithmic accuracy will be addressed by a variation of Q . Finally, we will investigate the uncertainty induced by the PDFs and the input value of $\alpha_s(M_Z)$.

3.3 Transverse momentum distribution up to NNLO+NNLL

In this section we present our results for the transverse momentum distribution of Higgs bosons produced in bottom quark annihilation. We study the impact of the newly evaluated terms at NNLO+NNLL by comparing them to NLO+NLL, both in absolute size and

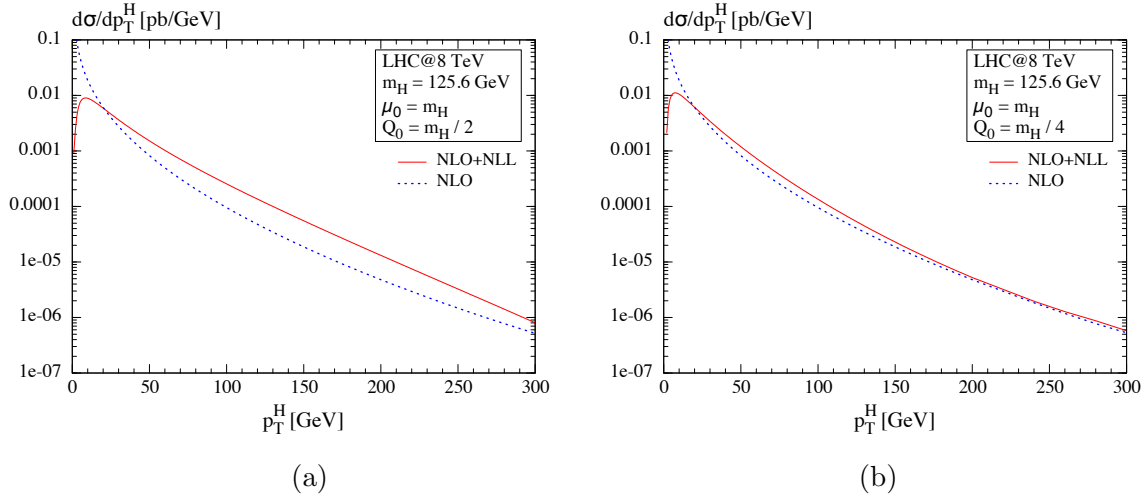


Figure 1: Transverse momentum spectrum at NLO (blue, dashed line) and at NLO+NLL (red, solid line) for (a) $Q = M/2$ and (b) $Q = M/4$. (Here and in the following plots, $m_H = M$ is the Higgs mass.)

in their theoretical uncertainty.

Fig. 1 shows the NLO+NLL together with the fixed-order NLO distribution for two values of the resummation scale Q : Fig. 1 (a) uses $Q = M/2$, which is the default value typically used in gluon fusion [16], while Fig. 1 (b) uses $Q = M/4$. Resummation aims at a valid description of the low- p_T region and indeed, the divergence at $p_T \rightarrow 0$ of the fixed-order result is turned into a regular behavior. Due to higher-order effects, the fixed-order and the resummed-matched curve may also significantly differ at $p_T \sim M$ [28], as is also observed for gluon fusion [19, 21].¹⁵ Fig. 1 shows that for bottom quark annihilation, this difference is significantly smaller for $Q = M/4$ than for $Q = M/2$. This observation motivates us to use $Q = Q_0 \equiv M/4$ as the central resummation scale choice also at NNLO+NNLL in the following.¹⁶ Nevertheless, for reference, we include results for $Q_0 = M/2$ in Appendix E.

At NNLO+NNLL, we find that the agreement between the fixed-order and the resummed-matched curve is further improved with respect to NLO+NLL, see Fig. 2 (a). This confirms that the difference between these two results at $p_T \sim M$ is due to higher-order effects. For $p_T \gtrsim 50$ GeV, the resummed-matched curve is practically on top of the fixed-order curve. We note in passing that the agreement between the fixed-order and the resummed-matched curve results from nontrivial cancellations among the individual partonic subchannels. For example, considering only the $b\bar{b}$ channel, there are still large differences between the two

¹⁵A standard option in HqT [16–18], for example, is to use an intersection point between the fixed-order and the resummed-matched curve in order to switch from the latter to the former towards large p_T .

¹⁶We thank an anonymous referee for this suggestion.

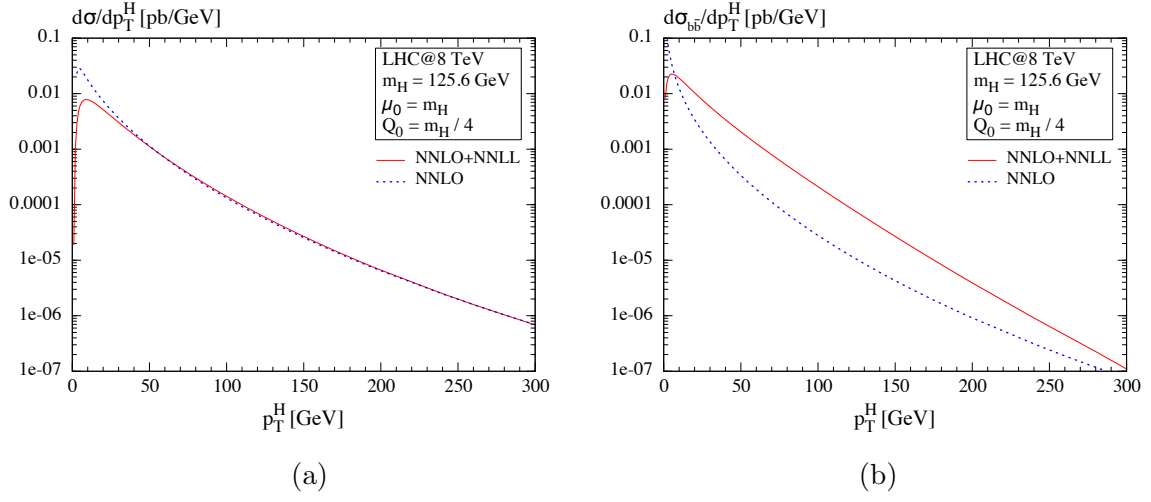


Figure 2: (a) Transverse momentum spectrum at NNLO (blue, dashed line) and at NNLO+NNLL (red, solid line) for the central scales; (b) only the $b\bar{b}$ channel for that quantity.

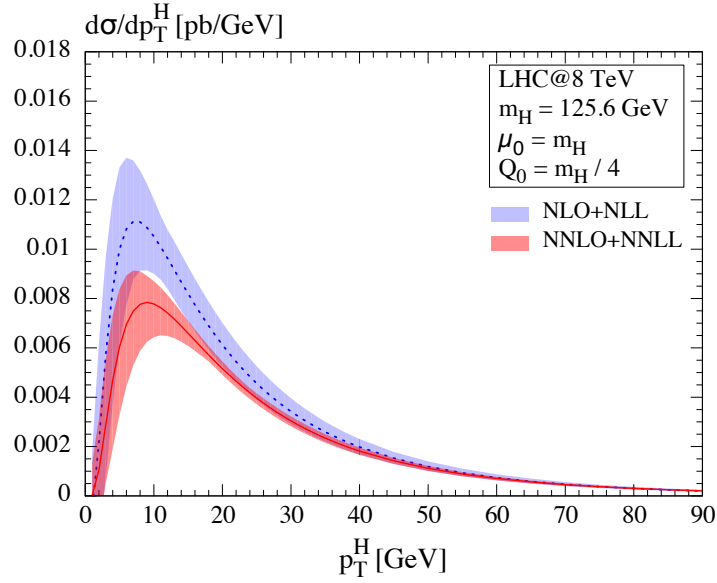


Figure 3: Resummed-matched p_T distribution at NLO+NLL (blue, dashed line) and NNLO+NNLL (red, solid line); lines: central scale choices; bands: uncertainty due to μ_F, μ_R -variation.

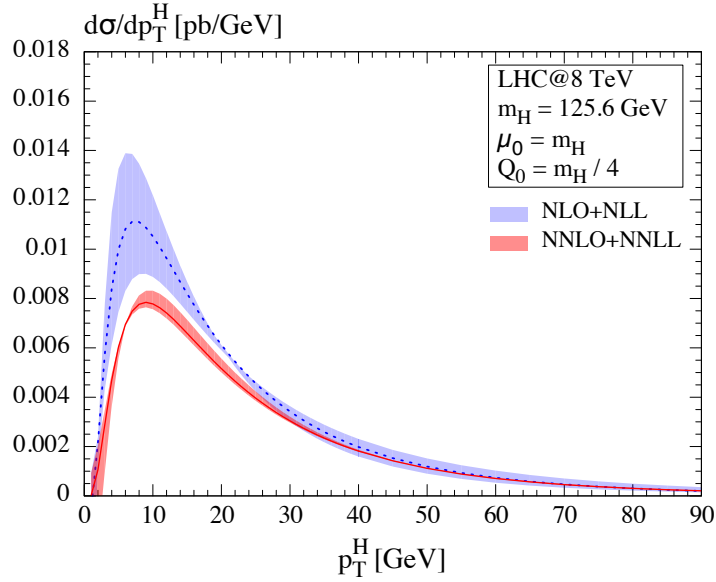


Figure 4: Resummed-matched p_T distribution at NLO+NLL (blue, dashed line) and NNLO+NNLL (red, solid line); lines: central scale choices; bands: uncertainty due to Q -variation.

curves, see Fig. 2 (b), which are, however, compensated by the other partonic channels. In conclusion, the NNLO+NNLL result is the first to combine the small and high- p_T region in a satisfactory way. This indicates its importance to obtain a distribution valid at all transverse momenta.

Let us now consider the effect of the higher orders on the dependence due to the renormalization and the factorization scale, while fixing the resummation scale at its default value, $Q = Q_0$. The bands in Fig. 3 correspond to an independent variation of μ_F and μ_R in the range $[\mu_0/2, 2\mu_0]$, while excluding the region where $\mu_F/\mu_R > 2$ and $\mu_F/\mu_R < 1/2$. Comparing the red NNLO+NNLL with the blue NLO+NLL band, a considerable decrease of the scale uncertainties is only observed for $p_T \gtrsim 20$ GeV, while in the region where resummation is crucial the error bands have a similar size.

Including higher orders in the logarithmic accuracy, one also expects a reduction of the dependence of the p_T distribution on the resummation scale. This is impressively confirmed in Fig. 4, which shows the cross sections at NLO+NLL and at NNLO+NNLL, where μ_F and μ_R are fixed at their default values (see Section 3.2). The bands are obtained by varying Q between $Q_0/2$ and $2Q_0$; the lines correspond to $Q = Q_0$. The variation of the cross section with respect to Q at NNLL is indeed significantly reduced with respect to NLL.

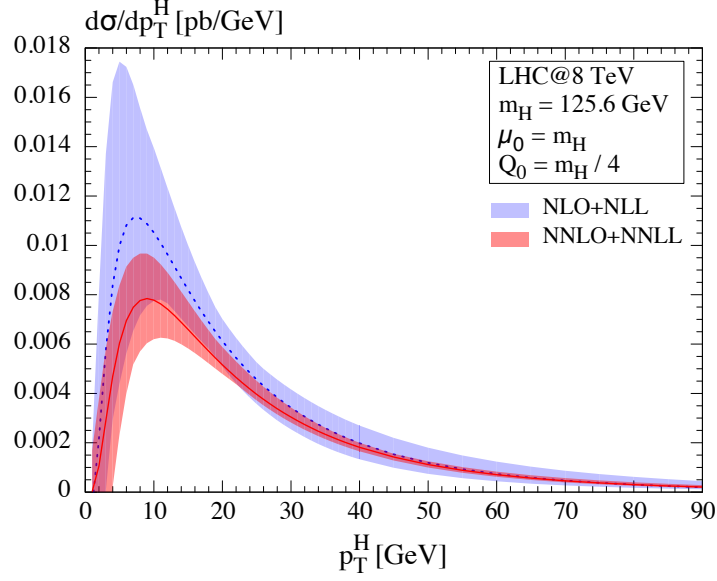


Figure 5: Resummed-matched p_T distribution at NLO+NLL (blue, dashed line) and NNLO+NNLL (red, solid line); lines: central scale choices; bands: uncertainty due to variation of all scales.

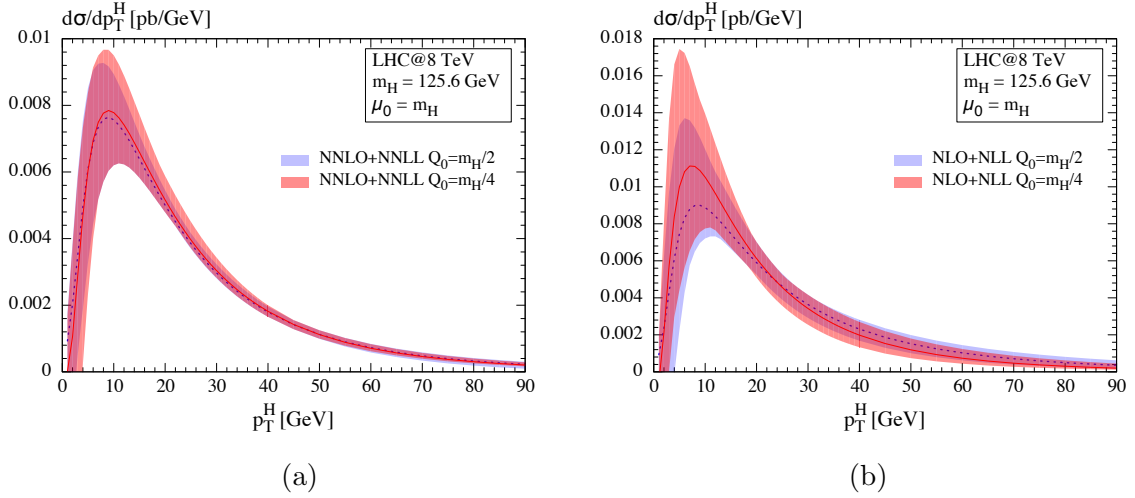


Figure 6: Transverse momentum spectrum using $Q_0 = M/4$ (red, solid line) and $Q_0 = M/2$ (blue, dashed line) as the central resummation scale. The bands indicate the theoretical uncertainty of the prediction as in Fig. 5. (a) NNLO+NNLL; (b) NLO+NLL.

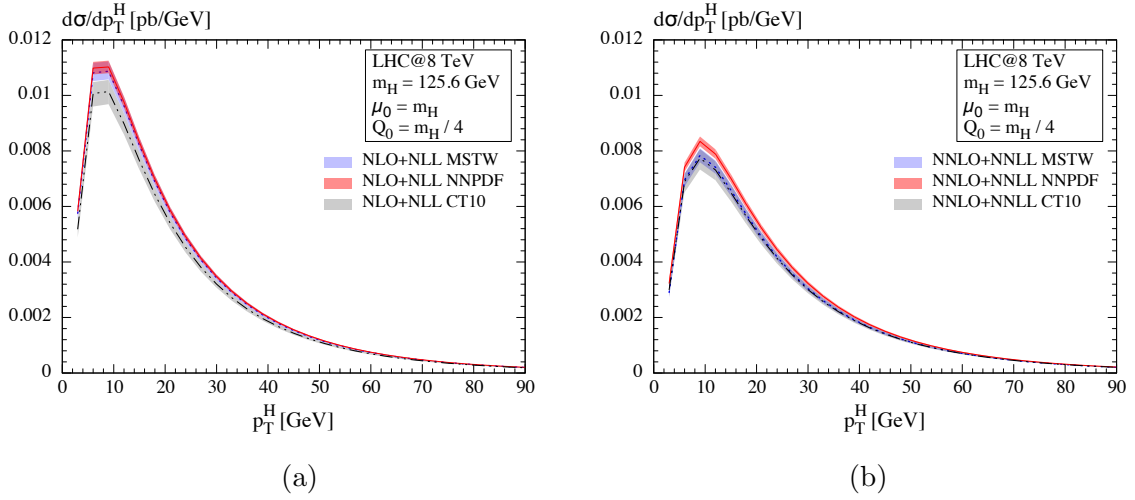


Figure 7: Resummed-matched p_T distribution at (a) NLO+NLL and (b) NNLO+NNLL for MSTW2008 (blue, dotted line), NNPDF2.3 (red, solid line) and CT10 (black, dash-dotted line); lines: central curves; bands: PDF+ α_s uncertainties at 68% CL.

Finally, Fig. 5 shows the result for an independent variation of all three scales within $Q \in [Q_0/2, 2Q_0]$ and $\mu_F, \mu_R \in [\mu_0/2, 2\mu_0]$, where again we exclude the regions $\mu_F/\mu_R > 2$ and $\mu_F/\mu_R < 1/2$. For all values of p_T , one observes a reduction of the uncertainty of the resummed-matched NNLO+NNLL cross section with respect to the one at NLO+NLL. The relative uncertainty at the maximum amounts to $+23/-23\%$ for the NNLL curve and $+48/-41\%$ at NLL.

The corresponding plots for 13 TeV are shown in Appendix D, Fig. 15-13. Qualitatively, the above statements also apply here, only the absolute cross section is larger.

At this point, we would like to get back to the central choice of the resummation scale. As we have argued before, $Q = M/4$ results in a good agreement in the high- p_T tail of the resummed-matched and fixed-order distribution, particularly at NNLO+NNLL. Furthermore, at this order, the choice of Q_0 only has a small impact on the distribution and the corresponding scale uncertainties at low p_T . This is shown in Fig. 6 (a), which compares the curves for $Q_0 = M/2$ (blue, dotted line) and $Q_0 = M/4$ (red, solid line) at NNLO+NNLL. The bands correspond to the variation of all scales as described above. The height of the peak differs only by about 3% between the two choices. The corresponding curves at NLO+NLL show a significantly larger difference, which is about 23% at the peak, see Fig. 6 (b). Let us note again that, for further comparison, plots for $Q_0 = M/2$ are given in Appendix E, Fig. 16-20.

Finally, let us discuss the uncertainties arising from the PDF and α_s choices. Besides

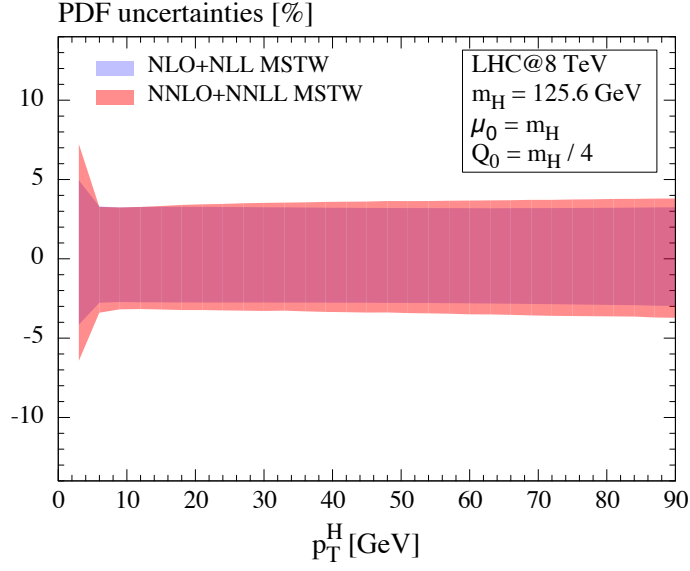


Figure 8: Relative uncertainties (68% CL) for the MSTW2008 PDF set of the resummed-matched p_T distribution at NLO+NLL (blue band) and NNLO+NNLL (red band).

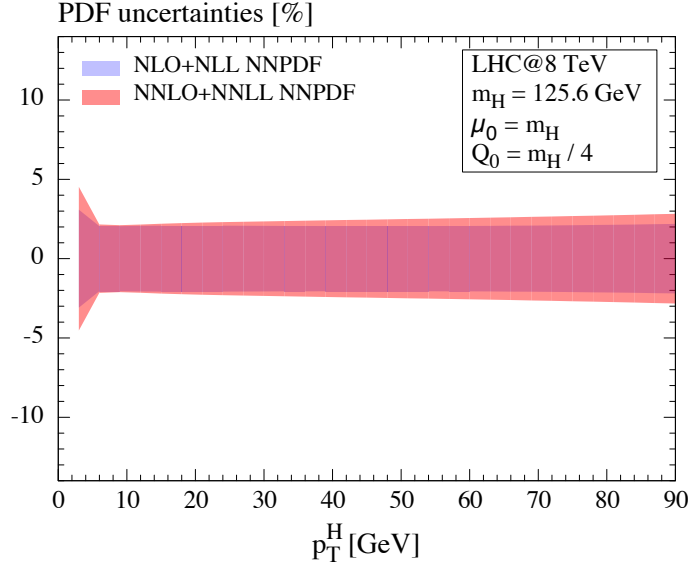


Figure 9: Relative uncertainties (68% CL) for the NNPDF2.3 PDF set of the resummed-matched p_T distribution at NLO+NLL (blue band) and NNLO+NNLL (red band).

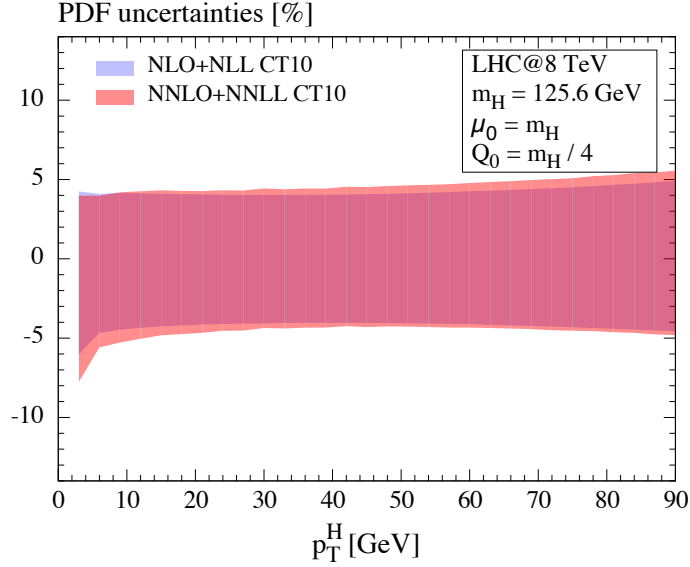


Figure 10: Relative uncertainties (68% CL) for the CT10 PDF set of the resummed-matched p_T distribution at NLO+NLL (blue band) and NNLO+NNLL (red band).

the importance for our calculation, this study is particularly interesting regarding the treatment of the bottom densities of the various PDF groups, given the fact that the $b\bar{b}H$ process in the 5FS is directly sensitive to the bottom densities. We consider three different PDF sets: MSTW2008, NNPDF2.3 and CT10. The combined PDF+ α_s uncertainties are determined following the recommendations of the corresponding PDF groups [46, 49, 50]. In contrast to MSTW and CTEQ, there is no central PDF set for NNPDF, which is why the central value is calculated as the mean value of all considered PDF members.

Fig. 7 compares the resummed-matched distributions obtained with the three PDF sets and their intrinsic uncertainties, for (a) NLO+NLL and (b) NNLO+NNLL accuracy. At NLO+NLL, the MSTW and NNPDF results are very consistent within their uncertainties, while the CTEQ band is right below the MSTW band. At NNLO+NNLL, on the other hand, the situation is the other way round: The bands of MSTW and CTEQ overlap, while the NNPDF band lies right on top of them. In both cases the biggest discrepancies are observed around the maximum of the distribution. This property may be due to the rather special role of the bottom densities which are not determined directly from experimental data, but are theoretically derived from the other parton densities and thus, are strongly dependent on their specific treatment in the different PDF groups. Furthermore, considering the relative uncertainties in Fig. 8 (MSTW), Fig. 9 (NNPDF) and Fig. 10 (CTEQ), we observe

PDF+ α_s uncertainties of similar size for the NLO and NNLO densities. This is expected since the PDF uncertainties arise only from the experimental input data. In fact, the NNLO uncertainties are slightly increased with respect to the NLO ones. In general the uncertainties of both cross sections NLO+NLL and NNLO+NNLL are rather small, $\lesssim 4\%$, $\lesssim 3\%$ and $\lesssim 5\%$ for MSTW, NNPDF and CTEQ, respectively.

The overall theoretical uncertainty on the cross section is clearly dominated by unphysical scales, in particular the factorization and renormalisation scale. It is therefore convenient to simply add the PDF+ α_s and scale uncertainty in quadrature.

4 Conclusions

The transverse momentum distribution of Higgs bosons produced in bottom quark annihilation has been presented through NNLO+NNLL accuracy, following the method of Ref. [16]. For this purpose, we calculated the missing second-order hard coefficient $H_b^{H,(2)}$ both numerically and analytically. By choosing an appropriate resummation scale, we obtain a resummed-matched distribution that matches well to the fixed-order prediction at large p_T already at NLO+NLL. At NNLO+NNLL, we observe excellent agreement between the resummed-matched and the fixed-order curve already above around 50 GeV. Our results therefore represent a precise prediction in the dominant region of low and intermediate values of transverse momenta.

Concerning the variation of the cross section with the unphysical scales, we observe a significant reduction when going from NLO+NLL to NNLO+NNLL. In fact, the extremely weak dependence of the NNLO+NNLL result on the resummation scale is remarkable. The PDF uncertainties are roughly of the same size at NLO+NLL and NNLO+NNLL, as it is expected from their purely experimental origin.

Our results should prove useful, in particular, in scenarios with enhanced bottom quark Yukawa coupling, such as supersymmetric or Two-Higgs-Doublet Models with large values of $\tan\beta$, but they may even be an important complement in the SM, especially once the statistics for Higgs events has improved. Not least of all, differential quantities in the $b\bar{b}H$ process provide good physical observables to study various parametrizations and implementations of b densities.

Acknowledgements. We would like to thank Giancarlo Ferrera and Massimiliano Grazzini for enlightening discussions, and J. Blümlein for helpful communication. The work of A.T. was supported in part by the University of Torino, the Compagnia di San Paolo, contract ORTO11TPXK, and DFG, contract HA 2990/5-1. M.W. was supported by BMBF, contract 05H12PXE, and by the European Commission through the FP7 Marie Curie Initial Training Network “LHCPhenoNet” (PITN-GA-2010-264564).

Appendix A Feynman diagrams

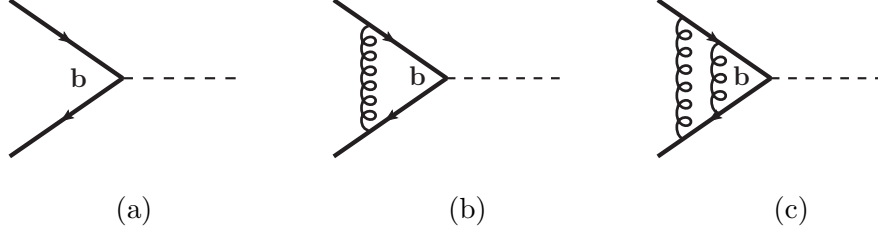


Figure 11: A sample of Feynman diagrams for $b\bar{b} \rightarrow H$ contributing to the NNLO cross section at $p_T = 0$; (a) LO, (b) one-loop and (c) two-loop.

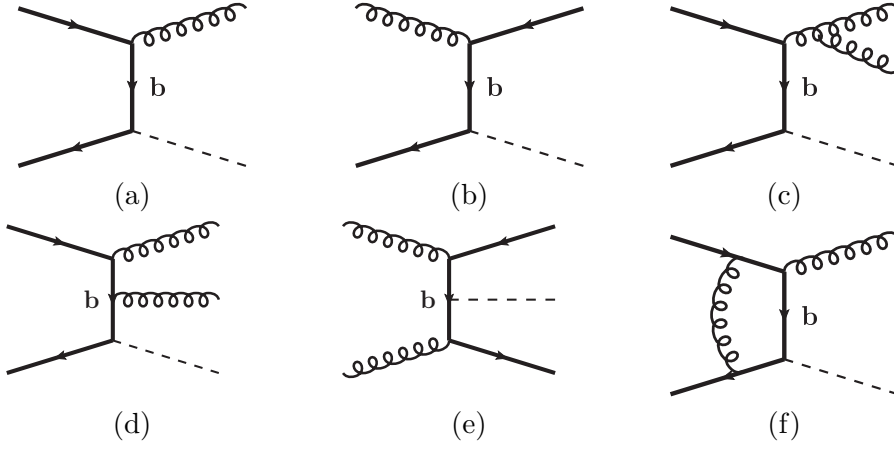


Figure 12: A sample of Feynman diagrams for $b\bar{b} \rightarrow H$ contributing to the NNLO cross section at $p_T > 0$; (a-b) single-real, (c-e) double-real, (f) mixed real-virtual.

Appendix B Hard-collinear coefficient with full scale dependence

In this appendix, we present expressions for the hard-collinear function to second order with complete scale dependence for the $b\bar{b}H$ process:

$$\begin{aligned}
 \mathcal{H}_{b\bar{b} \leftarrow ij}^{b\bar{b}H,(1)}(z) = & \delta(1-z) \delta_{bi} \delta_{\bar{b}j} \left[H_b^{H,(1)} - \left(B_b^{(1)} + \frac{1}{2} A_b^{(1)} \right) - 2\gamma_0 \ln(M^2/\mu_R^2) \right] \\
 & + \delta_{bi} C_{\bar{b}j}^{(1)}(z) + \delta_{\bar{b}j} C_{bi}^{(1)}(z) + \frac{1}{2} \left(\delta_{bi} P_{\bar{b}j}^{(0)}(z) + \delta_{\bar{b}j} P_{bi}^{(0)}(z) \right) \ln^3(M^2/Q^2),
 \end{aligned} \tag{28}$$

$$\begin{aligned}
\mathcal{H}_{b\bar{b}\leftarrow ij}^{b\bar{b}H,(2)}(z) = & \delta(1-z) \delta_{bi} \delta_{\bar{b}j} H_b^{H,(2)} + \delta_{bi} C_{\bar{b}j}^{(2)}(z) + \delta_{\bar{b}j} C_{bi}^{(2)}(z) + (C_{bi}^{(1)} \otimes C_{\bar{b}j}^{(1)})(z) \\
& + H_b^{h(1)} \left(\delta_{bi} C_{\bar{b}j}^{(1)}(z) + \delta_{\bar{b}j} C_{bi}^{(1)}(z) \right) + \delta(1-z) \delta_{bi} \delta_{\bar{b}j} \frac{1}{6} A_b^{(1)} \beta_0 \ln^3(M^2/Q^2) \\
& + \frac{1}{2} \left[\delta(1-z) \delta_{bi} \delta_{\bar{b}j} A_b^{(2)} + \beta_0 \Sigma_{b\bar{b}\leftarrow ij}^{(1;1)}(z) \right] \ln^2(M^2/Q^2) \\
& - \left[\delta(1-z) \delta_{bi} \delta_{\bar{b}j} \left(B_b^{(2)} + A_b^{(2)} \ln(M^2/Q^2) \right) \right. \\
& - \beta_0 \left(\delta_{bi} C_{\bar{b}j}^{(1)}(z) + \delta_{\bar{b}j} C_{bi}^{(1)}(z) \right) + \delta_{bi} \frac{1}{4} P_{\bar{b}j}^{(1)}(z) + \delta_{\bar{b}j} \frac{1}{4} P_{bi}^{(1)}(z) \left. \right] \ln(M^2/Q^2) \\
& + \frac{1}{4} \beta_0 \left(\delta_{bi} P_{\bar{b}j}^{(0)}(z) + \delta_{\bar{b}j} P_{bi}^{(0)}(z) \right) \ln^2(M^2/\mu_F^2) \\
& + \frac{1}{4} \left(\delta_{bi} P_{\bar{b}j}^{(1)}(z) + \delta_{\bar{b}j} P_{bi}^{(1)}(z) \right) \ln(M^2/\mu_F^2) - \mathcal{H}_{b\bar{b}\leftarrow ij}^{b\bar{b}H,(1)}(z) \beta_0 \ln(M^2/\mu_F^2) \\
& + \frac{1}{2} \sum_{i',j'} \left[\mathcal{H}_{b\bar{b}\leftarrow ij}^{b\bar{b}H,(1)}(z) + \delta(1-z) \delta_{bi'} \delta_{\bar{b}j'} H_b^{H,(1)} + \delta_{bi'} C_{\bar{b}j'}^{(1)}(z) + \delta_{\bar{b}j'} C_{bi'}^{(1)}(z) \right] \\
& \times \left\{ \frac{1}{2} \left(\delta_{i'i} P_{j'j}^{(0)}(z) + \delta_{j'j} P_{i'i}^{(0)}(z) \right) \ln(Q^2/\mu_F^2) - \delta(1-z) \delta_{i'i} \delta_{j'j} \right. \\
& \times \left[\left(B_b^{(1)} + \frac{1}{2} A^{(1)} \ln(M^2/Q^2) \right) \ln(M^2/Q^2) + 2\gamma_0 \ln(M^2/\mu_R^2) \right] \left. \right\} \\
& - \delta(1-z) \delta_{bi} \delta_{\bar{b}j} \left[\gamma_0 \beta_0 \ln^2(M^2/\mu_R^2) + 2\gamma_1 \ln(M^2/\mu_R^2) \right],
\end{aligned} \tag{29}$$

where M denotes the Higgs mass, $\Sigma_{b\bar{b}\leftarrow ij}^{(1;1)}$ is defined in Eq. (64) of Ref. [16], and $P_{ij}^{(n)}(z)$ denotes the Altrelli-Parisi splitting functions. Their expressions can be found in Ref. [51], for example. The quark mass anomalous dimension enters due to the fact that the Born factor is proportional to the square of the bottom quark mass (see Eq. (5)) which is normalized in the $\overline{\text{MS}}$ scheme:

$$\begin{aligned}
\gamma_0 &= \frac{3}{4} C_F, \\
\gamma_1 &= \frac{1}{16} \left(\frac{3}{2} C_F^2 + \frac{97}{6} C_F C_A - \frac{10}{3} C_F T_F N_f \right),
\end{aligned} \tag{30}$$

while the power of α_s at LO vanishes.

Appendix C Mellin transforms

Mellin transforms of several transcendental functions which appear in two-loop calculations are reported for integer N in Ref. [52]. Ref. [53] gives a FORTRAN code that numerically approximates the analytic continuation of the moments of 25 basic functions¹⁷ termed $g(1, z), \dots, g(25, z)$ (see Section 3 of Ref. [53]). The resummation coefficients $C_N^{(1)}$ and $C_N^{(2)}$ can be expressed in terms of the moments of these 25 basic functions $g(1, N), \dots, g(25, N)$, and the analytic continuation of the single harmonic sums $S_k(N)$. Below, we give analytic expressions for Mellin transforms defined by

$$f(N) = \int_0^1 dz z^{N-1} f(z) \quad (31)$$

of some of the transcendental functions, true for complex N , which appear in the coefficients $C^{(2)}$ of our calculation. The general definition of the harmonic sums is given by

$$S_{k_1, \dots, k_m}(N) = \sum_{n_1=1}^N \frac{(\text{sign}(k_1))^{n_1}}{n_1^{|k_1|}} \dots \sum_{n_m=1}^{n_m-1} \frac{(\text{sign}(k_m))^{n_m}}{n_m^{|k_m|}}, \quad (32)$$

which are defined, of course, only for integer N and for $k_i \neq 0$. The analytic continuations are known for single sums and are expressed in terms of the digamma function $\psi(N) = \psi^{(0)}(N)$ and the polygamma functions $\psi^{(m)}(N)$. They are given by

$$\begin{aligned} S_k(N) &= (-1)^{k-1} \frac{1}{(k-1)!} \psi^{(k-1)}(N+1) + c_k^+, \\ S_{-k}(N) &= (-1)^{k-1+N} \frac{1}{(k-1)!} \beta^{(k-1)}(N+1) - c_k^-, \end{aligned} \quad (33)$$

where

$$\begin{aligned} \psi(N) &= \frac{1}{\Gamma(N)} \frac{d\Gamma(N)}{dN}, & \psi^{(m)}(N) &= \frac{d^m \psi(N)}{dN^m}, \\ \beta(N) &= \frac{1}{2} \left[\psi\left(\frac{N+1}{2}\right) - \psi\left(\frac{N}{2}\right) \right], & \beta^{(m)}(N) &= \frac{d^m \beta(N)}{dN^m} \end{aligned} \quad (34)$$

and

$$\begin{aligned} c_1^+ &= \gamma_E, & c_k^+ &= \zeta_k \equiv \zeta(k), \quad k \geq 2, \\ c_1^- &= \log 2, & c_k^- &= \left(1 - \frac{1}{2^{k-1}}\right) \zeta_k, \quad k \geq 2. \end{aligned} \quad (35)$$

¹⁷The formula for $g(11, N)$ in Eq. (30) of Ref. [53] contains a typo: The last term $\frac{1}{4} \ln^4 2$ should be replaced by $\frac{1}{8} \ln^4 2$. We would like to thank J. Blümlein for confirmation.

We obtained the following Mellin transforms by modifying some of the formulas in Ref. [52, 53] such that they become valid for complex N :

$$\ln(1+z) \rightarrow \frac{1}{2N} \left[S_1 \left(\frac{N-1}{2} \right) - S_1 \left(\frac{N}{2} \right) + 2 \log 2 \right] \quad (36)$$

$$\text{Li}_2(-z) \rightarrow \frac{1}{2N^2} \left[S_1 \left(\frac{N-1}{2} \right) - S_1 \left(\frac{N}{2} \right) + 2 \log 2 \right] - \frac{\zeta_2}{2N} \quad (37)$$

$$\begin{aligned} \ln(z) \ln(1+z) \rightarrow & -\frac{1}{2N^2} \left[S_1 \left(\frac{N-1}{2} \right) - S_1 \left(\frac{N}{2} \right) + 2 \log 2 \right] \\ & - \frac{1}{4N} \left[S_2 \left(\frac{N-1}{2} \right) - S_2 \left(\frac{N}{2} \right) \right] \end{aligned} \quad (38)$$

$$\begin{aligned} \text{Li}_3 \left(\frac{1-z}{1+z} \right) - \text{Li}_3 \left(-\frac{1-z}{1+z} \right) \rightarrow & \left(S_1 \left(\frac{N-1}{2} \right) - S_1 \left(\frac{N}{2} \right) \right) \\ & \times \frac{1}{8N} \left[\psi^{(1)} \left(\frac{N+1}{2} \right) - 4\psi^{(1)}(N+1) - \psi^{(1)} \left(\frac{N+2}{2} \right) + \pi^2 \right] \\ & + \frac{1}{4N} \left[\psi^{(1)} \left(\frac{N+1}{2} \right) - 4\psi^{(1)}(N+1) - \psi^{(1)} \left(\frac{N+2}{2} \right) \right] (S_1(N) + \ln 2) \\ & + \frac{1}{N} \left[g(3, N+1) - g(4, N+1) + g(18, N+1) - g(19, N+1) \right], \end{aligned} \quad (39)$$

$$\begin{aligned} \frac{\ln(1+z) \ln^2(z)}{1+z} \rightarrow & 2g(5, N) - 2g(6, N) - 2g(7, N) \\ & + (-1)^{-N} \left[-\frac{1}{2}\zeta_3 S_{-1}(N-1) + \frac{3}{2}\zeta_3 S_1(N-1) + 4S_{-4}(N-1) \right. \\ & - \frac{1}{2}\pi^2 S_{-2}(N-1) + 2S_{-3}(N-1)S_1(N-1) + 2S_{-2}(N-1)S_2(N-1) \\ & \left. + \frac{1}{6}\pi^2 S_2(N-1) - \frac{1}{2}\zeta_3 \ln(2) - \frac{\pi^4}{360} \right], \end{aligned} \quad (40)$$

$$\begin{aligned}
& \frac{1}{1+z} \left[\text{Li}_3 \left(\frac{1}{1+z} \right) - \frac{1}{6} \ln^3(1+z) \right] \rightarrow \\
& \frac{1}{192} \left[\psi^{(0)} \left(\frac{N}{2} \right) \left(-24g \left(18, \frac{N}{2} \right) + 24g(19, N) - 9\zeta_3 + \pi^2(6\gamma + \ln(16)) \right) \right. \\
& - \psi^{(0)} \left(\frac{N+1}{2} \right) \left(-24g \left(18, \frac{N+1}{2} \right) + 24g(19, N) - 9\zeta_3 + \pi^2(6\gamma + \ln(16)) \right) \\
& - 4\pi^2 g(1, N) - 144g(5, N) + 192g(6, N) + 144g(7, N) + 96g(8, N) + 48g(10, N) \\
& + 96g(11, N) + 48g(12, N) + 24g \left(20, \frac{N}{2} \right) - 24g \left(20, \frac{N+1}{2} \right) + 24g \left(21, \frac{N}{2} \right) \\
& - 24g \left(21, \frac{N+1}{2} \right) + 24 \left(-\gamma g \left(18, \frac{N}{2} \right) + \gamma g \left(18, \frac{N+1}{2} \right) + \ln(4) g(4, N) \right. \\
& + 4(\psi^{(0)}(N) + \gamma)(g(3, N) - g(4, N)) \left. \right) + 9\psi^{(1)} \left(\frac{N}{2} \right) \psi^{(0)} \left(\frac{N}{2} \right)^2 \\
& - 12\psi^{(2)} \left(\frac{N}{2} \right) \psi^{(0)} \left(\frac{N}{2} \right) + 3\psi^{(1)} \left(\frac{N+1}{2} \right) \psi^{(0)} \left(\frac{N}{2} \right)^2 + 6\pi^2 \psi^{(0)}(N) \psi^{(0)} \left(\frac{N}{2} \right) \\
& + 6\psi^{(0)} \left(\frac{N+1}{2} \right) \psi^{(1)} \left(\frac{N}{2} \right) \psi^{(0)} \left(\frac{N}{2} \right) + 24\gamma \psi^{(1)} \left(\frac{N}{2} \right) \psi^{(0)} \left(\frac{N}{2} \right) \\
& - 6\psi^{(0)} \left(\frac{N+1}{2} \right) \psi^{(1)} \left(\frac{N+1}{2} \right) \psi^{(0)} \left(\frac{N}{2} \right) - 12\psi^{(0)}(N)^2 \psi^{(1)} \left(\frac{N+1}{2} \right) \\
& + 48\psi^{(2)}(N) \psi^{(0)} \left(\frac{N}{2} \right) - 6\pi^2 \psi^{(0)}(N) \psi^{(0)} \left(\frac{N+1}{2} \right) + 12\psi^{(0)}(N)^2 \psi^{(1)} \left(\frac{N}{2} \right) \\
& - 3\psi^{(0)} \left(\frac{N+1}{2} \right)^2 \psi^{(1)} \left(\frac{N}{2} \right) + 48\psi^{(0)}(N) \psi^{(0)} \left(\frac{N+1}{2} \right) \psi^{(1)}(N) \\
& - 9\psi^{(0)} \left(\frac{N+1}{2} \right)^2 \psi^{(1)} \left(\frac{N+1}{2} \right) - 24\gamma \psi^{(0)} \left(\frac{N+1}{2} \right) \psi^{(1)} \left(\frac{N+1}{2} \right) \\
& - 48\psi^{(0)} \left(\frac{N+1}{2} \right) \psi^{(2)}(N) + 12\psi^{(0)} \left(\frac{N+1}{2} \right) \psi^{(2)} \left(\frac{N+1}{2} \right) + \psi^{(3)} \left(\frac{N}{2} \right) \\
& - \psi^{(3)} \left(\frac{N+1}{2} \right) + 6(-\pi^2 - 2\ln^2(2) + \gamma(4\gamma + \ln(16))) \psi^{(1)} \left(\frac{N}{2} \right) + 6 \left[\pi^2 \right. \\
& + 2\ln^2(2) - \gamma(4\gamma + \ln(16)) \left. \right] \psi^{(1)} \left(\frac{N+1}{2} \right) + 48(\ln(2) - \gamma) \psi^{(1)}(N) \psi^{(0)} \left(\frac{N}{2} \right) \\
& + 24(\gamma + \ln(2)) \psi^{(0)}(N) \psi^{(1)} \left(\frac{N}{2} \right) + 48(\gamma - \ln(2)) \psi^{(0)} \left(\frac{N+1}{2} \right) \psi^{(1)}(N) \\
& - 24(\gamma + \ln(2)) \psi^{(0)}(N) \psi^{(1)} \left(\frac{N+1}{2} \right) - 12(\gamma + \ln(2)) \psi^{(2)} \left(\frac{N}{2} \right) \\
& \left. + 12(\gamma + \ln(2)) \psi^{(2)} \left(\frac{N+1}{2} \right) - 48\psi^{(0)}(N) \psi^{(1)}(N) \psi^{(0)} \left(\frac{N}{2} \right) \right], \tag{41}
\end{aligned}$$

where $\gamma = \gamma_E$. Note that in Eq. (40) factors of the form $(-1)^N$ cancel out completely upon insertion of the single harmonic sums in Eq. (33) .

Appendix D Results for 13 TeV

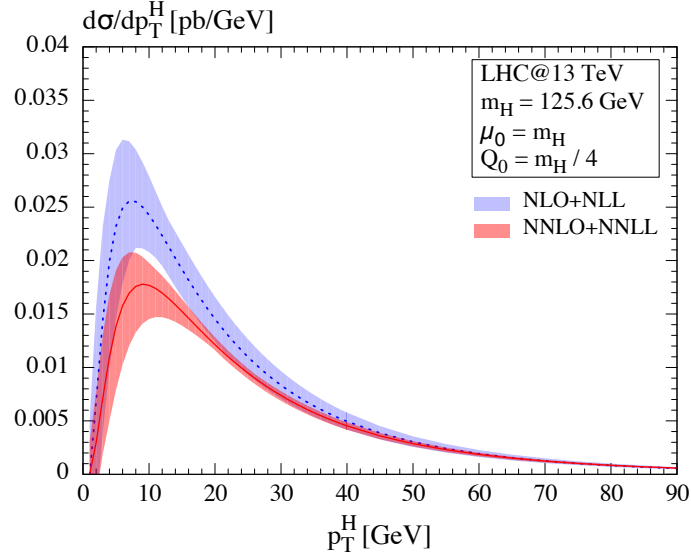


Figure 13: Resummed-matched p_T -distribution at NLO+NLL (blue, dashed line) and NNLO+NNLL (red, solid line); lines: central scale choices; bands: uncertainty due to μ_F, μ_R -variation. (Same as Fig. 3, but for $\sqrt{s} = 13$ TeV.)

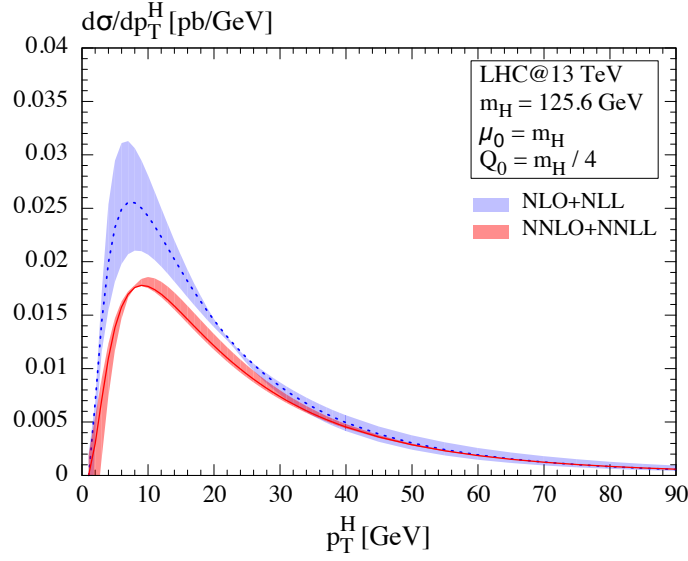


Figure 14: Resummed-matched p_T -distribution at NLO+NLL (blue, dashed line) and NNLO+NNLL (red, solid line); lines: central scale choices; bands: uncertainty due to Q -variation. (Same as Fig. 4, but for $\sqrt{s} = 13$ TeV.)

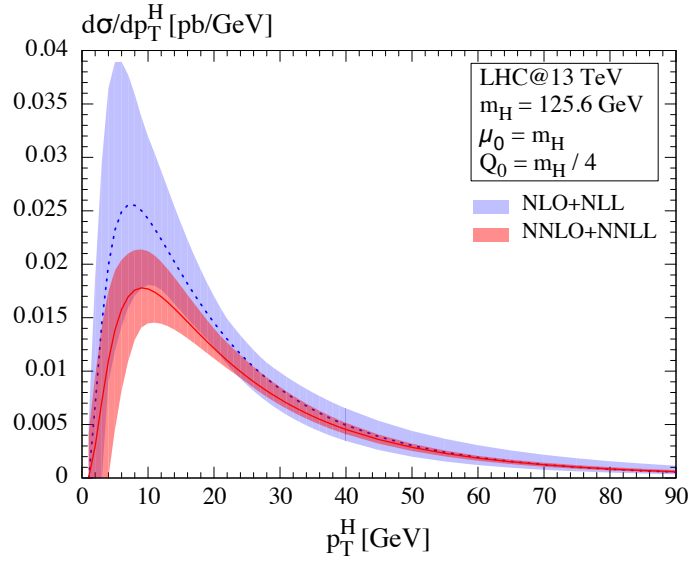


Figure 15: Resummed-matched p_T -distribution at NLO+NLL (blue, dashed line) and NNLO+NNLL (red, solid line); lines: central scale choices; bands: uncertainty due to variation of all scales. (Same as Fig. 5, but for $\sqrt{s} = 13$ TeV.)

Appendix E Results for $Q_0 = m_H/2$

In this appendix, we present the main results of the paper for a central resummation scale of $Q_0 = M/2$.

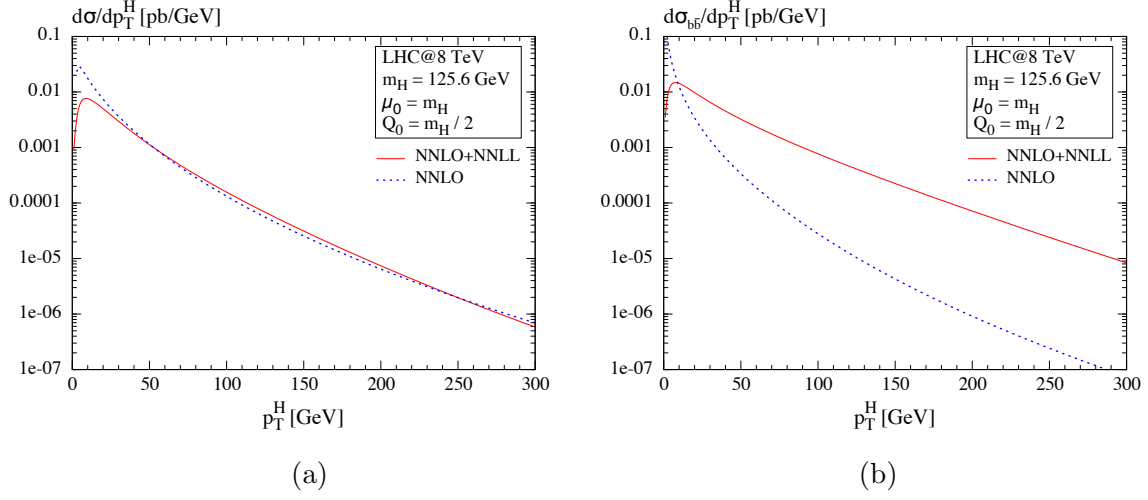


Figure 16: (a) Transverse momentum spectrum at NNLO (blue, dashed line) and at NNLO+NNLL (red, solid line) for the central scales; (b) only the $b\bar{b}$ channel for that quantity. (Same as Fig. 2, but for $Q_0 = M/2$.)

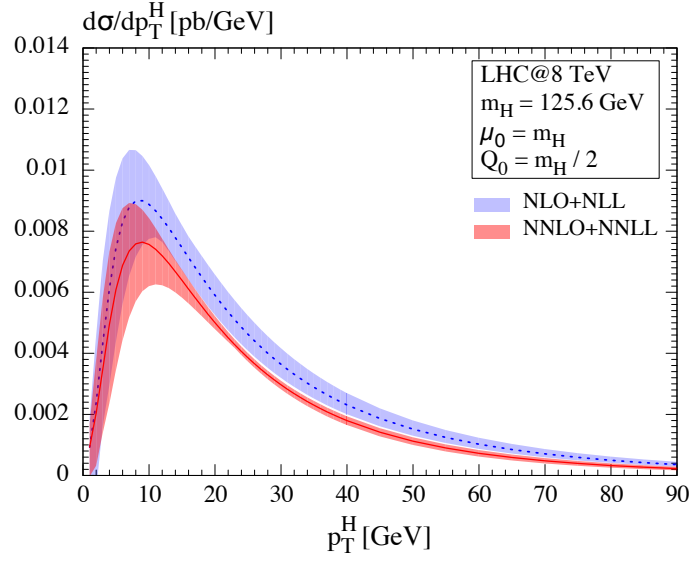


Figure 17: Resummed-matched p_T -distribution at NLO+NLL (blue, dashed) and NNLO+NNLL (red, solid); lines: central scale choices; bands: uncertainty due to μ_F, μ_R -variation. (Same as Fig. 3, but for $Q_0 = M/2$.)

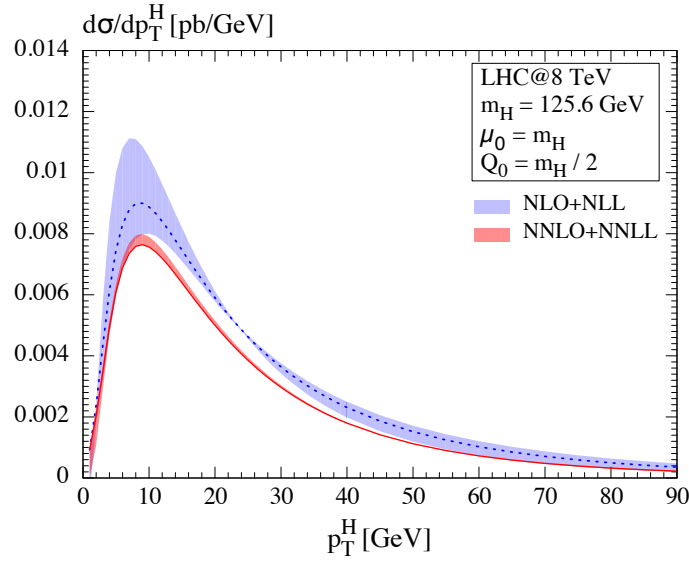


Figure 18: Resummed-matched p_T -distribution at NLO+NLL (blue, dashed line) and NNLO+NNLL (red, solid line); lines: central scale choices; bands: uncertainty due to Q -variation. (Same as Fig. 4, but for $Q_0 = M/2$.)

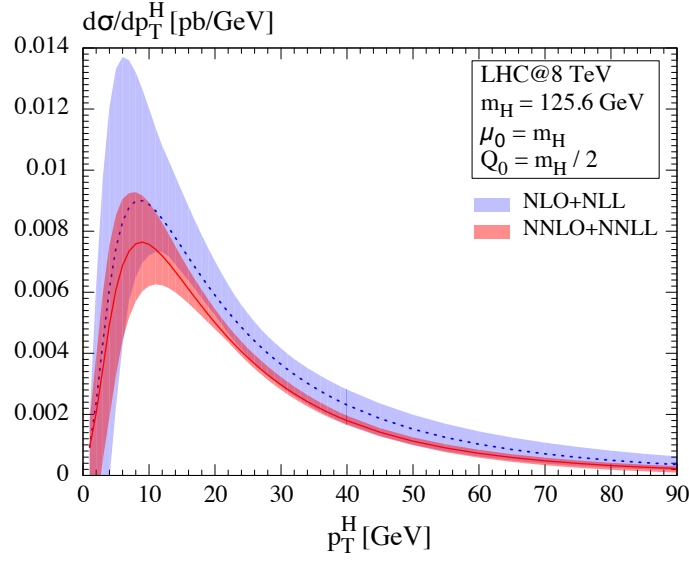


Figure 19: Resummed-matched p_T -distribution at NLO+NLL (blue, dashed line) and NNLO+NNLL (red, solid line); lines: central scale choices; bands: uncertainty due to variation of all scales. (Same as Fig. 5, but for $Q_0 = M/2$.)

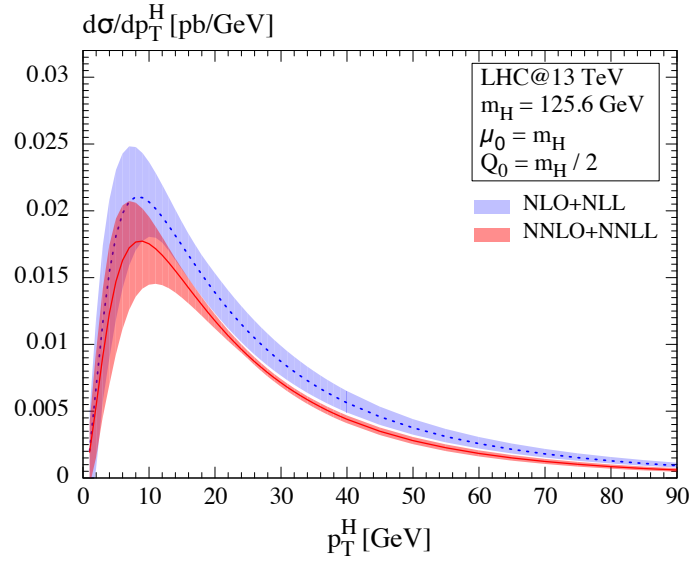


Figure 20: Resummed-matched p_T -distribution at NLO+NLL (blue, dashed line) and NNLO+NNLL (red, solid line); lines: central scale choices; bands: uncertainty due to μ_F, μ_R -variation. (Same as Fig. 13, but for $Q_0 = M/2$.)

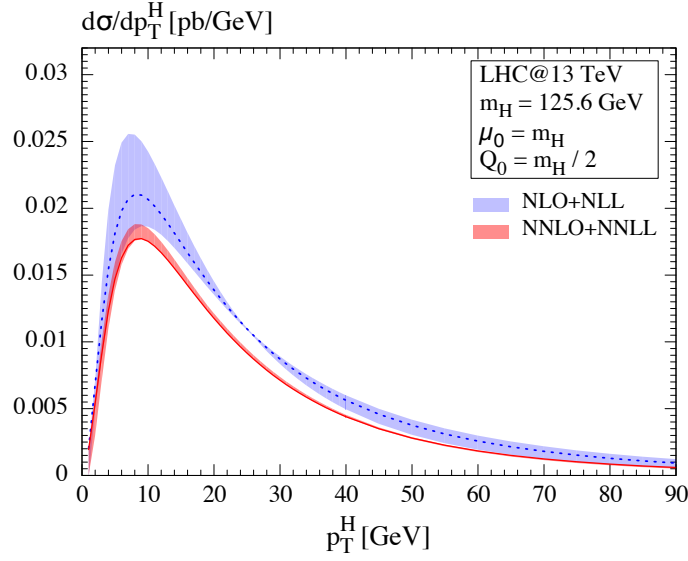


Figure 21: Resummed-matched p_T -distribution at NLO+NLL (blue, dashed line) and NNLO+NNLL (red, solid line); lines: central scale choices; bands: uncertainty due to Q -variation. (Same as Fig. 14, but for $Q_0 = M/2$.)

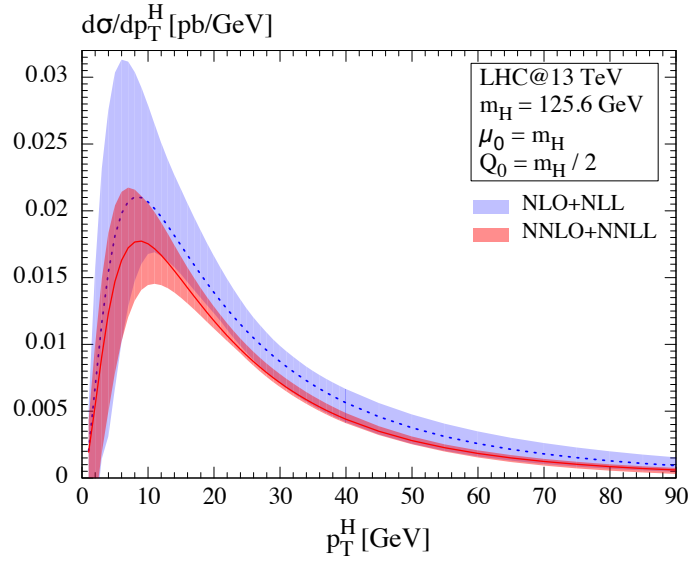


Figure 22: Resummed-matched p_T -distribution at NLO+NLL (blue, dashed line) and NNLO+NNLL (red, solid line); lines: central scale choices; bands: uncertainty due to variation of all scales. (Same as Fig. 15, but for $Q_0 = M/2$.)

References

- [1] S. Dittmaier *et al.* [LHC Higgs Cross Section Working Group Collaboration], arXiv:1101.0593 [hep-ph].
- [2] S. Dittmaier *et al.* [LHC Higgs Cross Section Working Group Collaboration], arXiv:1201.3084 [hep-ph].
- [3] S. Heinemeyer *et al.* [LHC Higgs Cross Section Working Group Collaboration], arXiv:1307.1347 [hep-ph].
- [4] M. Spira, Fortsch. Phys. **46** (1998) 203 [hep-ph/9705337].
- [5] S. Dittmaier, M. Krämer, and M. Spira, Phys. Rev. D **70** (2004) 074010 [hep-ph/0309204].
- [6] S. Dawson, C.B. Jackson, L. Reina and D. Wackerroth, Mod. Phys. Lett. A **21** (2006) 89 [hep-ph/0508293].
- [7] S. Dawson, C.B. Jackson, L. Reina and D. Wackerroth, Phys. Rev. D **69** (2004) 074027 [hep-ph/0311067].
- [8] R.V. Harlander and W.B. Kilgore, Phys. Rev. D **68** (2003) 013001 [hep-ph/0304035].
- [9] R. Harlander, M. Krämer and M. Schumacher, arXiv:1112.3478 [hep-ph].
- [10] R.V. Harlander and T. Neumann, Phys. Rev. D **88** (2013) 074015 [arXiv:1308.2225 [hep-ph]].
- [11] A. Azatov and A. Paul, JHEP **1401** (2014) 014 [arXiv:1309.5273 [hep-ph]].
- [12] C. Grojean, E. Salvioni, M. Schlaffer and A. Weiler, arXiv:1312.3317 [hep-ph].
- [13] D. de Florian, M. Grazzini and Z. Kunszt, Phys. Rev. Lett. **82** (1999) 5209 [hep-ph/9902483].
- [14] C.J. Glosser and C.R. Schmidt, JHEP **0212** (2002) 016 [hep-ph/0209248].
- [15] R.V. Harlander, T. Neumann, K. J. Ozeren and M. Wiesemann, JHEP **1208** (2012) 139 [arXiv:1206.0157 [hep-ph]].
- [16] G. Bozzi, S. Catani, D. de Florian and M. Grazzini, Nucl. Phys. B **737** (2006) 73 [hep-ph/0508068].
- [17] G. Bozzi, S. Catani, D. de Florian and M. Grazzini, Phys. Lett. B **564** (2003) 65 [hep-ph/0302104].

- [18] D. de Florian, G. Ferrera, M. Grazzini and D. Tommasini, JHEP **1111** (2011) 064 [arXiv:1109.2109 [hep-ph]].
- [19] H. Mantler and M. Wiesemann, Eur. Phys. J. C **73** (2013) 2467 [arXiv:1210.8263 [hep-ph]].
- [20] M. Grazzini and H. Sargsyan, JHEP **1309** (2013) 129 [arXiv:1306.4581 [hep-ph]].
- [21] A. Banfi, P.F. Monni, G. Zanderighi, *Quark masses in Higgs production with a jet veto*, arXiv:1308.4634.
- [22] A. Banfi, P. F. Monni, G. P. Salam and G. Zanderighi, Phys. Rev. Lett. **109** (2012) 202001 [arXiv:1206.4998 [hep-ph]].
- [23] R.V. Harlander, K.J. Ozeren and M. Wiesemann, Phys. Lett. B **693** (2010) 269 [arXiv:1007.5411 [hep-ph]].
- [24] K.J. Ozeren, JHEP **1011** (2010) 084 [arXiv:1010.2977 [hep-ph]].
- [25] R. Harlander and M. Wiesemann, JHEP **1204** (2012) 066 [arXiv:1111.2182 [hep-ph]].
- [26] S. Bühler, F. Herzog, A. Lazopoulos and R. Müller, JHEP **1207** (2012) 115 [arXiv:1204.4415 [hep-ph]].
- [27] J.M. Campbell, R.K. Ellis, F. Maltoni and S. Willenbrock, Phys. Rev. D **67** (2003) 095002 [hep-ph/0204093].
- [28] A. Belyaev, P.M. Nadolsky and C.-P. Yuan, JHEP **0604** (2006) 004 [hep-ph/0509100].
- [29] J.C. Collins, D.E. Soper and G.F. Sterman, Nucl. Phys. B **250** (1985) 199.
- [30] P.M. Nadolsky, N. Kidonakis, F.I. Olness and C.-P. Yuan, Phys. Rev. D **67** (2003) 074015 [hep-ph/0210082].
- [31] S. Catani, D. de Florian and M. Grazzini, Nucl. Phys. B **596** (2001) 299 [hep-ph/0008184].
- [32] S. Catani and M. Grazzini, Nucl. Phys. B **845** (2011) 297 [arXiv:1011.3918 [hep-ph]].
- [33] J. Kodaira and L. Trentadue, Phys. Lett. B **112** (1982) 66.
- [34] S. Catani, E. D’Emilio and L. Trentadue, Phys. Lett. B **211** (1988) 335.
- [35] T. Becher and M. Neubert, Eur. Phys. J. C **71** (2011) 1665 [arXiv:1007.4005 [hep-ph]].
- [36] C.T.H. Davies and W. J. Stirling, Nucl. Phys. B **244** (1984) 337.
- [37] S. Catani, L. Cieri, D. de Florian, G. Ferrera and M. Grazzini, Eur. Phys. J. C **72** (2012) 2195 [arXiv:1209.0158 [hep-ph]].

- [38] D. de Florian and M. Grazzini, Nucl. Phys. B **616** (2001) 247 [hep-ph/0108273].
- [39] V. Ravindran, Nucl. Phys. B **752** (2006) 173 [hep-ph/0603041].
- [40] S. Catani, L. Cieri, D. de Florian, G. Ferrera and M. Grazzini, Nucl. Phys. B **881** (2014) 414 [arXiv:1311.1654 [hep-ph]].
- [41] M. Wiesemann, Nucl. Phys. Proc. Suppl. **234** (2013) 25 [arXiv:1211.0977 [hep-ph]].
- [42] S. Frixione and B.R. Webber, JHEP **0206** (2002) 029 [hep-ph/0204244].
- [43] R. Frederix, S. Frixione, F. Maltoni and T. Stelzer, JHEP **0910** (2009) 003 [arXiv:0908.4272 [hep-ph]].
- [44] S. Frixione, F. Stoeckli, P. Torrielli and B.R. Webber, JHEP **1101** (2011) 053 [arXiv:1010.0568 [hep-ph]].
- [45] V. Hirschi, R. Frederix, S. Frixione, M.V. Garzelli, F. Maltoni and R. Pittau, JHEP **1105** (2011) 044 [arXiv:1103.0621 [hep-ph]].
- [46] A.D. Martin, W.J. Stirling, R.S. Thorne and G. Watt, Eur. Phys. J. C **63** (2009) 189 [arXiv:0901.0002 [hep-ph]].
- [47] S. Dawson, C.B. Jackson and P. Jaiswal, Phys. Rev. D **83** (2011) 115007 [arXiv:1104.1631 [hep-ph]].
- [48] S. Dittmaier, M. Krämer, A. Mück and T. Schlüter, JHEP **0703** (2007) 114 [hep-ph/0611353].
- [49] R.D. Ball *et al.*, Nucl. Phys. B **867** (2013) 244 [arXiv:1207.1303 [hep-ph]].
- [50] H.-L. Lai, M. Guzzi, J. Huston, Z. Li, P.M. Nadolsky, J. Pumplin and C.-P. Yuan, Phys. Rev. D **82** (2010) 074024 [arXiv:1007.2241 [hep-ph]].
- [51] R.K. Ellis and W. Vogelsang, hep-ph/9602356.
- [52] J. Blümlein and S. Kurth, Phys. Rev. D **60** (1999) 014018 [hep-ph/9810241].
- [53] J. Blümlein, Comput. Phys. Commun. **133** (2000) 76 [hep-ph/0003100].